



LUND
UNIVERSITY



DYNAMIC ANALYSIS OF THE INTERACTION BETWEEN VEHICLE FLOOR PANELS AND INTERIOR CARPETS

Simulations and Measurements

JAKOB DIAS DOS SANTOS INGESSON

Structural
Mechanics

Master's Dissertation

DEPARTMENT OF CONSTRUCTION SCIENCES
DIVISION OF STRUCTURAL MECHANICS

ISRN LUTVDG/TVSM--19/5239--SE (1-62) | ISSN 0281-6679

MASTER'S DISSERTATION

DYNAMIC ANALYSIS OF THE INTERACTION BETWEEN VEHICLE FLOOR PANELS AND INTERIOR CARPETS

Simulations and Measurements

JAKOB DIAS DOS SANTOS INGESSON

Supervisors: Dr **PETER PERSSON**, Division of Structural Mechanics, LTH
and Dr **OLA FLODÉN**, Volvo Cars.

Examiner: Professor **PER-ERIK AUSTRELL**, Division of Structural Mechanics, LTH.

Copyright © 2019 Division of Structural Mechanics,
Faculty of Engineering LTH, Lund University, Sweden.

Printed by V-husets tryckeri LTH, Lund, Sweden, July 2019 (*PI*).

For information, address:

Division of Structural Mechanics,
Faculty of Engineering LTH, Lund University, Box 118, SE-221 00 Lund, Sweden.

Homepage: www.byggmek.lth.se

Acknowledgements

The master dissertation was carried out as a joint project at the Division of Structural Mechanics at the Faculty of Engineering (LTH), Lund University and at Volvo Car Corporation in Gothenburg.

I would like to thank my supervisor Dr. Peter Persson at LTH for his valuable input and guidance. I would also like to thank my supervisor Dr. Ola Flodén at Volvo Car Corporation, who has shown great enthusiasm and interest to my work. Without his encouragement and guidance, this work would not have been possible. Additionally, I would also like to thank all my colleagues in the Body NVH team at Volvo Car Corporation for their help and encouragement. Especially I would like to thank them for welcoming me and making me feel as a part of the group from the very first day.

Then, I would like to thank Agnes Broholm for encouraging me when my motivation was low, and for listening to me talk endlessly about panel and carpet vibrations the past months. Finally, I would like to extend my gratitude to all my friends that have been with me during all these years leading up to this point, for their love and support. Especially I would like to thank Alexander Kjellgren for both his friendship and for making the study time more enjoyable. Last I would like to thank my mother for her love and patience.

Gothenburg, June 2019

Jakob Dias Dos Santos Ingesson

Abstract

Floor panels of vehicles are known to radiate structure-borne sound into the vehicle compartment. To reduce the structure-borne sound, numerical models are used in the development of vehicles to evaluate different design options of the vehicle body. The panels are covered with carpets composed of foam and heavy layer of rubber, which causes challenges and complications when predicting interior sound.

In the current models used to predict sound, the carpets are modelled as non-structural mass added to the panels. It is believed that the heavy layer setup of the carpets leads to a sprung-mass resonance in the frequency of interest for structure-borne sound. This affects the dynamic behaviour and sound radiation of the floor panels. Further, the panels and carpets are believed to not be in full contact with each other, and the contact condition is assumed to vary among vehicles and over time. Therefore it is assumed that the current modelling strategy used to model floor panels is not able to predict the dynamic behaviour of the panels and carpets with sufficient accuracy. This leads to erroneous results and conclusions in the development of cars.

A step towards a modelling strategy capable of predicting interior noise levels with higher accuracy, is to understand the dynamic behaviour of panels and carpets. In this Master's dissertation, an example structure of a floor panel with carpet is studied experimentally and numerically. The effect of the carpet on the dynamic response in the panel, and the response in the panel compared to that in the heavy layer is investigated. It was found that a model with a simple linear-elastic solid representation of the carpet is able to represent the basic phenomena that govern the dynamic behaviour of panels and carpets. Although, further investigation is needed to achieve adequate correlation of the vibration levels and resonance frequencies. A sprung-mass resonance of the carpet was clearly observed in both measurements and numerical analyses. A significant effect of contact condition between panel and carpet was also found.

Contents

1	Introduction	1
1.1	Background	1
1.2	Aim and Objective	3
1.3	Method	4
1.4	Example Structure	4
2	Governing Theory	7
2.1	Continuum Formulation	7
2.2	Finite Element Formulation	8
2.3	Structural Dynamic Analysis	9
2.3.1	Free Vibration	9
2.3.2	Forced Harmonic Vibration	10
2.3.3	Damping	11
2.3.4	Frequency Response Function	12
2.3.5	Equivalent Radiated Power	12
2.4	Experimental Analysis	13
2.4.1	Hammer Impact Testing	13
2.4.2	Root Mean Square FRF	14
3	Numerical Pre-Test Analyses	15
3.1	Numerical Model of Example Structure	15
3.1.1	Modelling of Panel	16
3.1.2	Modelling of Carpet	17
3.1.3	Modelling of Interface	17
3.2	Vibrational Response of Panel and Carpet	18
3.2.1	Dynamic Behaviour in Different Frequency Ranges	18
3.2.2	Influence of Accelerometer Mass	20
3.2.3	Influence of Boundary Conditions	21
3.3	Frequency Response Function vs Equivalent Radiated Power	22
4	Experimental Analysis	25
4.1	Experimental Setup	25
4.2	Measurement Errors and Measurement Procedure	28
4.2.1	Measurement Procedure	29

4.2.2	Effect of Experimental Setup Parameters on Measured Behaviour	29
4.3	Measured Response Functions	34
4.3.1	Dispersion Study	36
4.3.2	Panel Without Carpet	36
4.3.3	Panel With Carpet	37
4.3.4	Heavy Layer	37
4.4	Experimental Results	38
4.4.1	Effect of Carpet on Panel Response	38
4.4.2	Panel vs Heavy Layer Response	40
4.4.3	Effect of Variations in Carpets	41
5	Correlation of Numerical and Experimental Results	43
5.1	Correlation of Panel Without Carpet	43
5.2	Correlation of Panel With Carpet	44
5.2.1	Glued Carpet	44
5.2.2	Non-Glued Carpet	45
5.3	Parametric Study	46
5.3.1	Stiffness of Carpet	46
6	Conclusions and Discussion	49
6.1	Main Observations	49
6.2	Discussion	50
6.2.1	Test Specimen	50
6.2.2	Evaluation of Measured Data	50
6.2.3	Accuracy of Numerical Model	51
6.2.4	Damping	52
6.2.5	Adding Stiffness by Gluing	52
6.3	Proposals for Future Work	53
A	Repeatability	57

1. Introduction

1.1 Background

Customers of automotive vehicles have become more sensitive to, and aware of, noise and vibrations [1]. Additionally, interior noise levels are often deemed as an indicator of overall vehicle quality. Therefore the noise, vibration and harshness (NVH) attributes are important to consider when developing a car today.

A main source of interior noise in vehicles is structure-borne noise, which originates from different types of dynamic loading of the vehicle body. The dynamic loading can, for instance, be loads from tyre–road interaction, electrical installations or the powertrain. The dynamic loading gives rise to vibrations that are transmitted through the vehicle body resulting in sound radiation from the panels of the vehicle body into the interior. One significant source of interior structure-borne sound are the floor panels of the car, which are shown in Figure 1.1. To reduce the sound radiation from these panels, the panels are covered with carpets that consist of foam with a heavy layer of rubber on top. The main purpose of the heavy layer is to act as a double wall together with the panel. Isolating high frequency airborne sound. However, the interaction between floor panels and carpets affects the structure-borne sound, and this effect is not fully understood. This causes challenges and complications when modelling noise transmission and predicting noise levels in the development of a vehicle.

In the development of a model simplifications and assumptions are made. There is a risk that these simplifications and assumptions lead to a model incapable of representing the physical phenomena that governs the interior noise. This can lead to erroneous decisions in the vehicle development. A thorough understanding of the physical phenomena governing the dynamic behaviour of the system is therefore needed.

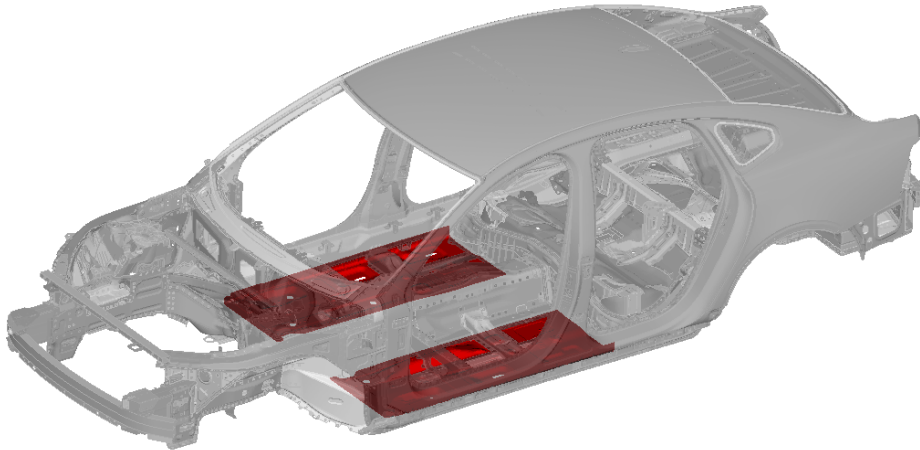


Figure 1.1: The body structure of a car currently in production. The floor panels are shown in red.

The master's dissertation focuses on the vibro-mechanical behaviour of floor panels and carpets. It should be seen as a step towards a deeper understanding of the physical phenomena that govern sound radiation from floor panels in vehicles. This is, in turn, a step towards accurate prediction of acoustic pressure in vehicles.

The carpets are often modelled as non-structural mass (NSM) on the panels, which is a rough simplification. This only consider the added mass effect of the carpet on the panel. A less rough simplification would be to describe the foam in the carpet as a spring and the heavy layer as a mass. It is reasonable to assume that such a model is able to represent the behaviour of the system, with higher accuracy than a model where the carpet is modelled with NSM. By modelling foam and heavy layer as spring and mass, it is reasonable to assume a frequency-dependent behaviour. More particularly, one can assume three types of behaviour: 1) the carpet acts as an added mass in low frequencies, 2) the heavy layer is resonant in somewhat higher frequencies and 3) the heavy layer is vibration isolated in even higher frequencies. This frequency-dependent behaviour is hereinafter referred to as the *expected behaviour*. If this assumption is correct, it is reasonable to assume that a model with a linear-elastic solid element representation of the carpet would be able to represent the expected behaviour.

Other studies have been investigating the behaviour of similar systems as the panel-carpet system in question [2][3][4][5]. The studies confirm the hypothesis that

the carpet behaves as a added mass in low frequencies. They also indicate that modelling trim items composed of foam (carpets for instance) with a poro-elastic material model gives a good representation of the measured behaviour in regard to air-borne sound transmission. However, the measurements in all but one of the cited studies are made on systems where the carpets have been glued to the panels. Glued carpets have the advantages that the connection between panel and carpet is relatively well-defined, which simplifies modelling of the system.

When the carpets are not glued to the panels but solely laid on top of them, it causes uncertainty of how much and what parts of the carpet that are in contact with the panels. Furthermore, it is likely that the contact condition varies between vehicles, and over time. It is therefore of interest to investigate how the arbitrary variations in contact between the carpet and panel influence the behaviour of the carpet-panel system.

1.2 Aim and Objective

As discussed in Chapter 1.1, carpets are often modelled as NSM in analyses of structure-borne sound. This is likely to result in poor accuracy of the predictions. In order to increase the accuracy it is of interest to develop a model which is able to represent the physical phenomena that governs the dynamic behaviour of the floor panels and carpets. To achieve such a model, the dynamic behaviour of, and the interaction between, floor panels and carpets needs to be better understood. By procuring a better understanding of the dynamic behaviour of floor panels and carpets, it is possible to evaluate the hypothesis that modelling the carpet with linear-elastic solids will increase the accuracy of the predictions.

The work done in the master's dissertation aims at increasing the knowledge regarding the dynamic behaviour of floor panels and carpets, to improve the modelling strategies used to predict acoustic pressure in vehicles. More precisely, is this a step towards the development of a modelling strategy that is able to represent all relevant physical phenomena necessary to predict the noise radiation from floor panels with adequate accuracy.

The objectives are to:

- Carrying out measurements of the dynamic behaviour of, and the interaction between, floor panels and carpets in different frequency ranges.
- Carrying out measurements of how contact conditions between floor panels and carpets affect the dynamic behaviour and interaction.
- Provide recommendations for analytical modelling of carpets in different frequency ranges.

1.3 Method

In the dissertation, the vehicle floor panels and carpets are represented by an example structure. The example structure is based on a floor panel and carpet from a currently produced vehicle. The example structure is further explained in Chapter 1.4.

The work done in the dissertation can be divided into three parts. The first part is numerical pre-test analyses. Here, numerical analyses were performed to give an indication of what was to be expected from the measurement results. The model analysed was a rough model of the example structure, created from a CAD model. The analyses included both free vibration analyses and forced harmonic response analyses. The results from the analyses were also used in the design of the experimental setup. The influence of the position of the suspension and the effect of accelerometer mass was evaluated, among other things. The analyses are further explained in Chapter 3.

The second part is the experimental analysis. Here, measurements were performed on specimen of the example structure. The measurements included a dispersion study of the panels without carpets, response measurements on panels with and without carpets, and response measurements of panels and heavy layers. The measurements are further explained in Chapter 4.

The third part is the correlation of numerical and experimental results. Here different modelling strategies of the panel-carpet system were evaluated. This was done by evaluating the correlation between numerical results and measurement results. Also, the sensitivity to variations in material parameters was evaluated. This is explained in detail in Chapter 5.

1.4 Example Structure

The example structure that was the used in the dissertation was a cut out from a floor panel and carpet from a currently produced vehicle. The panels were cut from the left floor panel of the vehicle. The part of the panel chosen for the study is the part under the feet of the left rear passenger and is shown in Figure 1.2. This part was chosen because it had a large contact surface against the carpet, and that the cuts were possible to make in the physical panel without damaging the panel. Since the floor panels were machine manufactured it was believed that they were close to identical, before cutting them. The panels are made of 0.6 mm sheet metal.

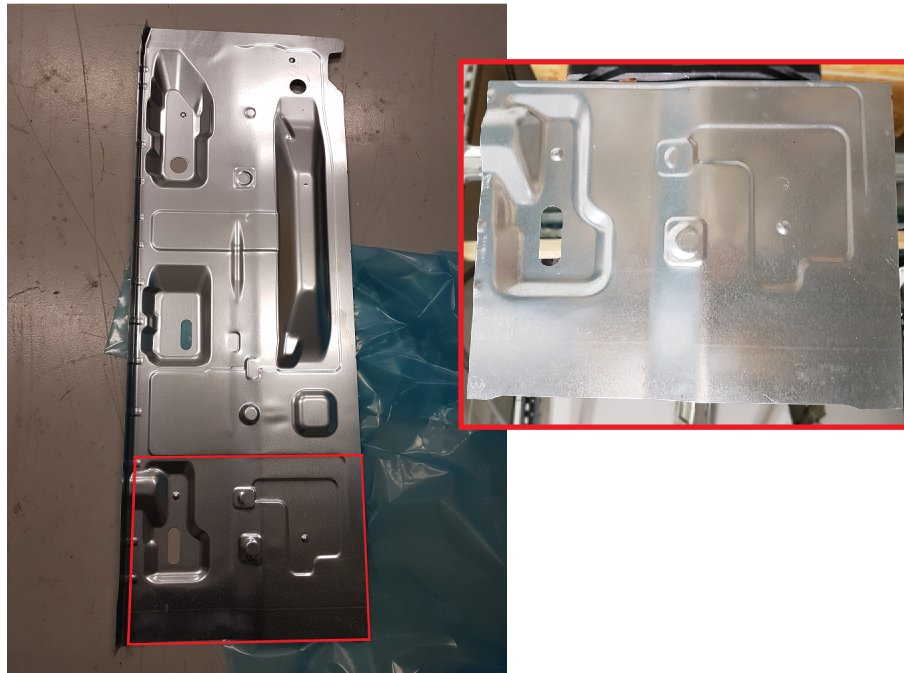


Figure 1.2: Photographs of the full size floor panel and the cut-out from the panel.

The carpets are composed of foam, rubber and a soft fabric, in this specific order from bottom to top. The carpets with its layers are shown in Figure 1.3. The thickness of the foam layer varies over the area from approximately 20 mm to 30 mm. The side of the foam that is in contact with the panel are shaped to follow the geometry of the panels. The other side, which the heavy layer are attached to, follows the geometry of the heavy layer, which is almost flat. The heavy layer is made out of rubber and is approximately 2 mm thick across the whole area. The soft fabric is glued to the heavy layer and is approximately 3 mm thick.

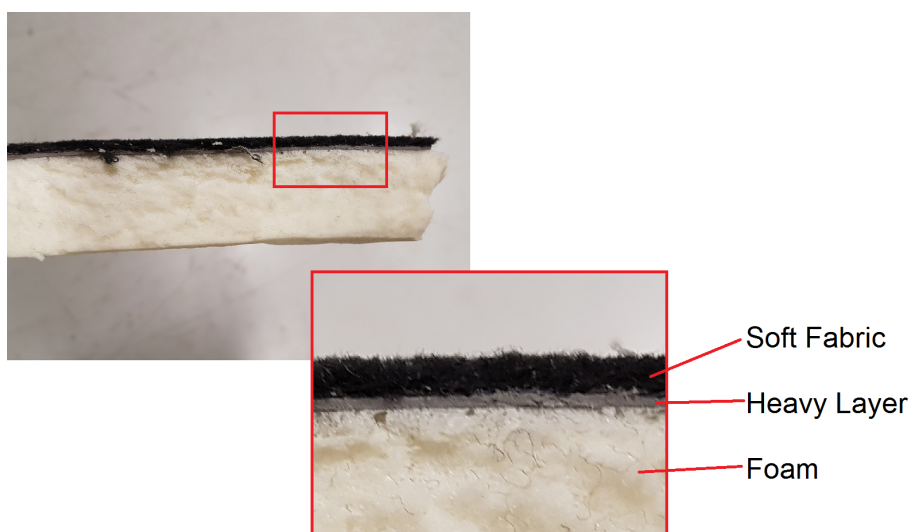


Figure 1.3: Section of a carpet where the different layers are visible.

The part of the full size carpet that was chosen, for the example structure, was a bit smaller than the panel cut-outs. This can be seen in Figure 1.4. The reason for this was that the part of the full size carpet that was in direct contact with the panel cut-out was not big enough to cover the whole panel cut-out. Instead of a smaller panel cut-out, which would require two more sides to be cut and thereby increasing the possibility of introducing geometry deviations between the panel cut-outs, it was decided that smaller carpet cut-outs was the best solution.

To be able to attached the accelerometer to the heavy layer, the layer of soft fabric on top of the heavy layer had to be removed. The spots where the soft fabric was removed is shown in Figure 1.4.

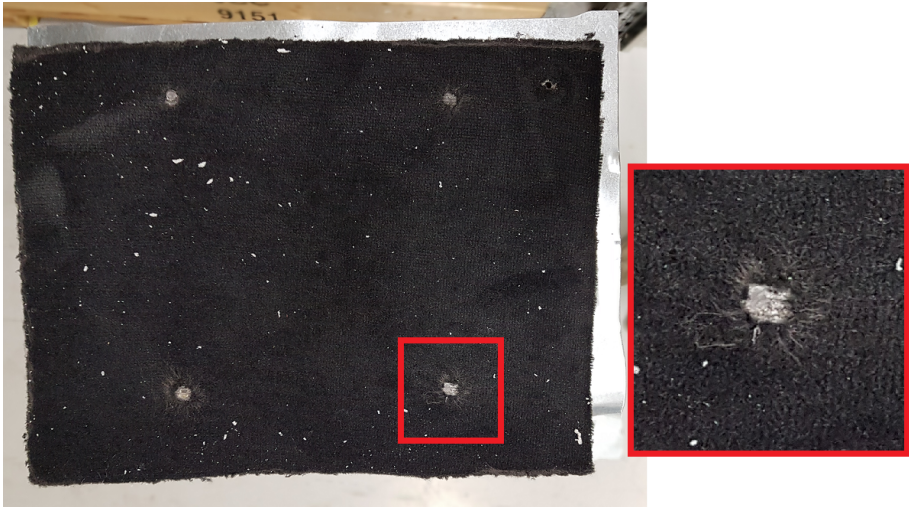


Figure 1.4: Top view of panel with carpet. A spot where the fabric has been removed to allow for placement of accelerometer on the heavy layer is visible.

2. Governing Theory

In this chapter, the theoretical background to both numerical and experimental methods used in the dissertation is presented.

2.1 Continuum Formulation

The equation of motion for a body, occupying the domain V can be derived as [6]

$$\sigma_{ij,j} + b_i = \rho \ddot{u}_i \quad (2.1)$$

where $\sigma_{ij,j}$ is the differentiated *stress tensor* σ_{ij} with respect to the coordinates x_j , b_i is the body force tensor, ρ is the density and \ddot{u}_i is the acceleration vector. Assuming that the displacement gradients $u_{i,j}$ are small the *strain tensor* is given by

$$\varepsilon_{ij} = \frac{1}{2}(u_{i,j} + u_{j,i}) \quad (2.2)$$

If the constitutive law, describing the relation between stresses and strains, is assumed to be linear the stress-strain relation is given by

$$\sigma_{ij} = D_{ijkl}\varepsilon_{kl} \quad (2.3)$$

where D_{ijkl} is the *elastic stiffness tensor*. A surface traction vector t_i is defined at the surface S of the domain V . The traction vector is given by

$$t_i = \sigma_{ij}n_j \quad (2.4)$$

where n_j is the outer unit normal vector of the surface S . Boundary conditions are given as

$$\begin{aligned} u_i &= u_i^{bc} & \text{on } S^u \\ t_i &= t_i^{bc} & \text{on } S^t \end{aligned} \quad (2.5)$$

where known displacements are prescribed on S^u , and known surface tractions are prescribed on S^t . Together, S^u and S^t make up the complete boundary S .

2.2 Finite Element Formulation

In order to solve the differential equations derived in the previous section, numerical methods are used. In structural mechanics the Finite Element Method (FE method) is widely use. The FE formulation allows the differential equations to be written as a system of algebraic equations. By solving the system of equations an approximation of the differential equations can be found.

The first step in deriving the FE formulation is to derive the weak formulation of (2.1). The equation of motion (2.1) is multiplied by an arbitrary vector v_i and integrated over the volume to obtain

$$\int_V v_i(\sigma_{ij,j} + b_i - \rho\ddot{u}_i)dV \quad (2.6)$$

By rewriting the (2.6) and using the divergence theorem we obtain

$$\int_V \rho v_i \ddot{u}_i dV + \int_V v_{i,j} \sigma_{ij} dV = \int_S v_i t_i dS + \int_V v_i b_i dV \quad (2.7)$$

Defining the quantity ε_{ij}^v as $\varepsilon_{ij}^v = \frac{1}{2}(v_{i,j} + v_{j,i})$ and utilising the symmetry of σ_{ij} the following expression can be derived

$$v_{i,j} \sigma_{ij} = \frac{1}{2}(v_{i,j} \sigma_{ij} + v_{j,i} \sigma_{ji}) = \frac{1}{2}(v_{i,j} \sigma_{ij} + v_{i,j} \sigma_{ji}) = \varepsilon_{ij}^v \sigma_{ij} \quad (2.8)$$

It is now possible to rewrite (2.7) by use of (2.8) obtaining the weak form of (2.1)

$$\int_V \rho v_i \ddot{u}_i dV + \int_V \varepsilon_{ij}^v \sigma_{ij} dV = \int_S v_i t_i dS + \int_V v_i b_i dV \quad (2.9)$$

From the weak formulation of the equation of motion it is possible to derive the FE formulation. First, the quantities in (2.9) are rewritten in matrix notation

$$\boldsymbol{\varepsilon}^v = \begin{bmatrix} \varepsilon_{11}^v \\ \varepsilon_{22}^v \\ \varepsilon_{33}^v \\ 2\varepsilon_{12}^v \\ 2\varepsilon_{13}^v \\ 2\varepsilon_{23}^v \end{bmatrix}; \quad \boldsymbol{\sigma} = \begin{bmatrix} \sigma_{11} \\ \sigma_{22} \\ \sigma_{33} \\ \sigma_{12} \\ \sigma_{13} \\ \sigma_{23} \end{bmatrix}; \quad \ddot{\mathbf{u}} = \begin{bmatrix} \ddot{u}_1 \\ \ddot{u}_2 \\ \ddot{u}_3 \end{bmatrix}; \quad \mathbf{v} = \begin{bmatrix} v_1 \\ v_2 \\ v_3 \end{bmatrix}; \quad \mathbf{t} = \begin{bmatrix} t_1 \\ t_2 \\ t_3 \end{bmatrix}; \quad \mathbf{b} = \begin{bmatrix} b_1 \\ b_2 \\ b_3 \end{bmatrix}$$

whereon the (2.9) can be written as

$$\int_V \rho \mathbf{v}^T \ddot{\mathbf{u}} dV + \int_V (\boldsymbol{\varepsilon}^v)^T \boldsymbol{\sigma} dV = \int_S \mathbf{v}^T \mathbf{t} dS + \int_V \mathbf{v}^T \mathbf{b} dV \quad (2.10)$$

Introduction of the approximation of the displacement vector \mathbf{u}

$$\mathbf{u} = \mathbf{N} \mathbf{a} \quad (2.11)$$

where \mathbf{N} is the global shape functions and \mathbf{a} is the nodal displacements, and choosing the weight vector \mathbf{v} in accordance with Galerkin's method, the following quantities can be introduced

$$\ddot{\mathbf{u}} = \mathbf{N} \ddot{\mathbf{a}}; \quad \boldsymbol{\varepsilon} = \mathbf{B} \mathbf{a}; \quad \mathbf{v} = \mathbf{N} \mathbf{c}; \quad \boldsymbol{\varepsilon}^v = \mathbf{B} \mathbf{c}; \quad \mathbf{B} = \frac{d\mathbf{N}}{dx_i}$$

where \mathbf{c} is an arbitrary column matrix. It is now possible to rewrite (2.10) as

$$\mathbf{c}^T \left[\left(\int_V \rho \mathbf{N}^T \mathbf{N} dV \right) \ddot{\mathbf{a}} + \int_V \mathbf{B}^T \boldsymbol{\sigma} dV - \int_S \mathbf{N}^T \mathbf{t} dS - \int_V \mathbf{N}^T \mathbf{b} dV \right] = 0 \quad (2.12)$$

considering a linear constitutive law the following quantities can be defined

$$\mathbf{M} = \int_V \rho \mathbf{N}^T \mathbf{N} dV ; \quad \mathbf{K} = \int_V \mathbf{B}^T \mathbf{D} \mathbf{B} dV ; \quad \mathbf{f} = \int_S \mathbf{N}^T \mathbf{t} dS + \int_V \mathbf{N}^T \mathbf{b} dV$$

where \mathbf{M} is referred to as the mass matrix, \mathbf{K} is referred to as the stiffness matrix and \mathbf{f} is referred to as the force vector. Taking advantage of that \mathbf{c} is arbitrary (2.10) can be rewritten as

$$\mathbf{M} \ddot{\mathbf{a}} + \mathbf{K} \mathbf{a} = \mathbf{f} \quad (2.13)$$

2.3 Structural Dynamic Analysis

The system in (2.13) is a so called multi-degree of freedom (MDoF) system. This section considers free vibrations and forced harmonic vibrations of a MDoF system. Also, damping and frequency response functions are treated.

2.3.1 Free Vibration

Assume a undamped MDoF system experiencing free-vibration, i.e. no external loads acting on the structure. The system is given by

$$\mathbf{M} \ddot{\mathbf{a}}(t) + \mathbf{K} \mathbf{a}(t) = \mathbf{0}. \quad (2.14)$$

Solutions to this (2.14) can be found by assuming the the harmonic solution

$$\mathbf{a}(t) = \hat{A} e^{i\omega t} \boldsymbol{\Phi}, \quad (2.15)$$

where \hat{A} is the complex amplitude, i is the imaginary unit, ω is the angular frequency and $\boldsymbol{\Phi}$ is a constant vector. By differentiating (2.15) and inserting into (2.14), the eigenvalue problem is given as

$$(\mathbf{K} - \omega^2 \mathbf{M}) \boldsymbol{\Phi} = \mathbf{0}. \quad (2.16)$$

Solutions to (2.16) can be found by solving

$$\det(\mathbf{K} - \omega^2 \mathbf{M}) = 0. \quad (2.17)$$

A MDof system with n number of DoFs will have n number of solutions, $\omega_j = \omega_1, \dots, \omega_n$. These solutions are the eigenfrequencies of the system. Each eigenfrequency has corresponding eigenmodes, or mode shapes, $\boldsymbol{\Phi}_j$ that describes the vibrational pattern of the mode. The eigenmodes can be determined by inserting the eigenfrequency of the mode in (2.16). The set of eigenmodes form an orthogonal

basis which results in that the solution to (2.14) can be described by the sum of the eigenmodes:

$$\mathbf{a}(t) = \sum_{j=1}^n q_j(t) \Phi_j, \quad (2.18)$$

where

$$q_j(t) = \hat{q}_j e^{i\omega_j t}. \quad (2.19)$$

The complex amplitude \hat{q}_j of Φ_j is determined by the initial conditions.

2.3.2 Forced Harmonic Vibration

The steady state response of a system is the response that appears after the initial transient response when the system is subjected to a harmonic force. Assume that a undamped MDof system is the subject to a harmonic force. This can be described by

$$\mathbf{M}\ddot{\mathbf{a}}(t) + \mathbf{K}\mathbf{a}(t) = \hat{\mathbf{f}}e^{i\omega t}, \quad (2.20)$$

where $\hat{\mathbf{f}}$ is a constant complex vector that describes the load distribution. The solution to (2.20) is given by the complimentary solution and the particular solution. The complimentary solution is given by (2.18) and is dependent of the initial conditions. The particular solution, which is not dependent on the initial condition, can be derived by assuming

$$\mathbf{a}(t) = \hat{\mathbf{a}}e^{i\omega t}, \quad (2.21)$$

where $\hat{\mathbf{a}}$ is a time-constant complex vector. By this assumption it is possible to write (2.20) as

$$(-\omega^2 \mathbf{M} + \mathbf{K})\hat{\mathbf{a}} = \hat{\mathbf{f}}. \quad (2.22)$$

Pre-multiplying this expression with the eigenmodes Φ_k^T , where $k = 1, \dots, n$, and modally decomposing $\hat{\mathbf{a}}$ as

$$\hat{\mathbf{a}} = \sum_{j=1}^n \hat{r}_j(t) \Phi_j, \quad (2.23)$$

the following expression can be derived:

$$-\omega^2 \sum_{j=1}^n \Phi_k^T \mathbf{M} \Phi_j \hat{r}_j + \sum_{j=1}^n \Phi_k^T \mathbf{K} \Phi_j \hat{r}_j = \Phi_k^T \hat{\mathbf{f}}. \quad (2.24)$$

Considering that the eigenmodes are orthogonal, the scalar products $\Phi_k^T \mathbf{M} \Phi_j$ and $\Phi_k^T \mathbf{K} \Phi_j$ are only non-zero if $k = j$. This results in n uncoupled systems, given by

$$-\omega^2 \bar{m}_j \hat{r}_j + \bar{k}_j \hat{r}_j = \bar{f}_j, \quad (2.25)$$

where

$$\bar{m}_j = \Phi_j^T \mathbf{M} \Phi_j, \quad \bar{k}_j = \Phi_j^T \mathbf{K} \Phi_j, \quad \bar{f}_j = \Phi_j^T \hat{\mathbf{f}}, \quad (2.26)$$

for $j = 1, \dots, n$. The n uncoupled systems, each describes the amplitude of an eigenmode which are given by

$$\hat{r}_j = \frac{\bar{f}_j}{\bar{k}_j} \frac{1}{1 - (\omega/\omega_j)^2} \quad (2.27)$$

where

$$\omega_j = \sqrt{\frac{\bar{k}_j}{\bar{m}_j}}. \quad (2.28)$$

Through the equations derived above, the particular solution to (2.20) can be obtained as

$$\mathbf{a}(t) = e^{i\omega t} \sum_{j=1}^n \frac{\bar{f}_j}{\bar{k}_j} \frac{1}{1 - (\omega/\omega_j)^2} \Phi_j. \quad (2.29)$$

The solution to the MDof system given by (2.20) is thus given by the sum of the complimentary solution (2.18) and the particular solution (2.29), as

$$\mathbf{a}(t) = \sum_{j=1}^n \hat{q}_j e^{i\omega_j t} \Phi_j + e^{i\omega t} \sum_{j=1}^n \frac{\bar{f}_j}{\bar{k}_j} \frac{1}{1 - (\omega/\omega_j)^2} \Phi_j. \quad (2.30)$$

2.3.3 Damping

Damping includes several mechanisms that dissipates energy from a vibrating system in different ways. Energy can be dissipated by repeated elastic straining of materials or internal losses in materials, for instance. Damping can be added in a numerical model by introducing the damping matrix \mathbf{C} in the equation of motion as

$$\mathbf{M}\ddot{\mathbf{a}}(t) + \mathbf{C}\dot{\mathbf{a}}(t) + \mathbf{K}\mathbf{a}(t) = \mathbf{f}(t). \quad (2.31)$$

It is not possible to determine the damping matrix of a structure in the same manner as the stiffness matrix is determined. The reasons for this is, for instance, that the damping properties of materials are not well established and the energy dissipation in joints and micro cracks are hard to measure and determine. Instead, the measured modal damping ratios of a structure are used to construct the damping matrix. The damping matrix can be constructed in multiple ways which can be categorised into two groups, classical and non-classical damping matrices. Classical damping matrices are possible to modally diagonalize which the non-classical damping matrices are not. Since the classical damping matrices can be diagonalized, a MDof system can be decomposed into uncoupled single degree-of-freedom (SDof) equations. This is beneficial when solving the numerical system. The damped SDoF system is derived by making the same assumption as in (2.21) and modally decomposing $\hat{\mathbf{a}}$ as in (2.23), acquiring

$$-\omega^2 \bar{m}_j \hat{r}_j + i\omega \gamma_j \hat{r}_j + \bar{k} \hat{r}_j = \hat{f}, \quad (2.32)$$

where $\gamma_j = \Phi_j^T \mathbf{C} \Phi_j$ and the other quantities are the same as introduced in (2.26). Introducing the damping ratio ζ_j as

$$\zeta_j = \frac{\gamma_j}{2\bar{m}_j \omega_j}, \quad (2.33)$$

where ω_j is the eigenfrequency of eigenmode j , introduced in (2.28). It is now possible to rewrite (2.32) as

$$-\omega^2 \bar{m}_j \hat{r}_j + 2i\zeta_j \bar{m}_j \omega_j \omega \hat{r}_j + \bar{k} \hat{r}_j = \hat{f}, \quad (2.34)$$

and solving for \hat{r}_j to obtain

$$\hat{r}_j = \frac{\hat{f}_j}{\omega_j^2} \frac{1}{1 - (\omega/\omega_j)^2 + 2i\zeta_j(\omega/\omega_j)} \quad (2.35)$$

which can be inserted into (2.23) to obtain the particular solution to the damped system (2.31). Since the system is damped, the transient response, which is described by the complementary solution, will be damped out. Hence, the response can be described by the particular solution.

2.3.4 Frequency Response Function

A frequency response function (FRF) describes the complex vibration amplitude in a point due to an excitation by a harmonic unit load in another (or the same) point. The FRF describes this relation in the frequency domain. The FRFs of a system excited by a harmonic unit load, can be derived by rewriting (2.31) as

$$\hat{\mathbf{a}} = (\mathbf{K} + i\omega\mathbf{C} - \omega^2\mathbf{M})^{-1}\hat{\mathbf{f}} = \mathbf{H}(\omega)\hat{\mathbf{f}}, \quad (2.36)$$

where the FRFs of the system are expressed by $\mathbf{H}(\omega)$. By modal decomposition of the system, each FRF can be described as

$$H_j = \frac{1}{\omega_j^2} \frac{1}{1 - (\omega/\omega_j)^2 + 2i\zeta(\omega/\omega_j)} \quad (2.37)$$

This FRF describes the output as a displacement, i.e. the FRF describes displacement as a function of force. This format of the FRF is also referred to as compliance. Often in the automotive industry, the output is described by velocity. This format is called mobility and is given by

$$H_j = \frac{1}{\omega_j^2} \frac{i\omega}{1 - (\omega/\omega_j)^2 + 2i\zeta(\omega/\omega_j)} \quad (2.38)$$

FRFs can also be calculated from experimentally measurements of a structure. Consider a structure excited by a force in DoF m , and where the the vibration response is measured i DoF n . Let $x_m(t)$ be the measured discrete time signal of the force and $y_n(t)$ the measured discrete time signal of the vibration response. The discrete time signals can then be expressed in the frequency domain by fast Fourier transformation (FFT). Let $X_m(\omega)$ and $Y_n(\omega)$ be the time signals expressed in the frequency domain. The FRF is then given by

$$H_{mn}(\omega) = \frac{Y_n(\omega)}{X_m(\omega)}, \quad (2.39)$$

2.3.5 Equivalent Radiated Power

The Equivalent Radiated Power (ERP) can be used as an upper estimate of the true radiated sound power in the high frequency range. In the low frequency range, as in

this application, the ERP can be used as a measure of vibrational activity [7]. The ERP is a weighted sum of the squared normal velocities on a surface and given by

$$\text{ERP}(\omega) = \frac{1}{2}\rho_0c \int_A |v_n(\omega)|^2 dA \quad (2.40)$$

where ρ_0 denotes the initial density of the fluid and c denotes the speed of sound in the fluid.

2.4 Experimental Analysis

Experimental analysis is typically used to determine modal parameters of a structure. By exciting the structure with a known force and measuring the response it is possible to determine modal parameters such as resonance frequencies, damping ratios and mode shapes of the structure. Usually the structure is excited by a shaker or an impact hammer. Which method that is used depends on the type of structure that is the subjects of the analysis. For light small structures, such as the example structure analysed in the dissertation, hammer impact testing was used.

2.4.1 Hammer Impact Testing

The hammers that are used features an integrated force sensor which registers the force of the impact. The tip of the hammer is usually interchangeable, which allows for excitations with different characteristics. A rule of thumb is that a softer tip, such as a rubber tip, excites the lower frequencies more. A harder tip, such as a metal tip, is able to excite the higher frequencies more.

The frequency content and the level of energy of the input force are important factors in obtaining a measurement with high quality. An excitation should have a high energy level so that the signal-to-noise ratio in the measurements is high. Otherwise the repeatability of the measurements will suffer. However, if the input force is too high there is a risk of triggering non-linear behaviour. This will also have a negative effect on the repeatability. The frequency content of the input force should be as linear as possible to avoid a low signal-to-noise ratio in some frequency ranges. Otherwise the repeatability will suffer in these frequencies.

The response of the structure is usually measured with accelerometers or a laser doppler vibrometer. In the measurements performed in the dissertation, accelerometers were used. The relationship between the input force and the measured response can be described by a frequency response function (FRF), as described in Chapter 2.3.4. As FRF describes the relationship between two points, it is typically used to gain an understanding of how a structure transmits vibrations. However, a FRF can also be used for estimating modal parameters by different curve fitting techniques. It is also possible to visualise the mode shapes of the structure. This is done by measuring multiple FRFs. The FRF contains information regarding the relation of amplitude and the phase difference between input and output.

Furthermore, hammer impact testing can be divided into two types: roving hammer and roving accelerometer. In the roving hammer impact testing, one or

more accelerometers are placed on the structure. The structure is then excited in multiple points, one after another. In roving accelerometer impact testing the structure is excited in the same point and the accelerometer is moved around. A combination of the two can also be used. Which one of the methods that are used depends on the structure that is analysed.

2.4.2 Root Mean Square FRF

To get a more general measure of the response of a surface, the response is measured in multiple points. A generalised mean is then calculated from the measured FRFs. The generalised mean of the FRFs describes the general response of the surface and is given by

$$M_p(f) = \left(\frac{1}{n} \sum_{i=1}^n FRF_i^p(f) \right)^{\frac{1}{p}} \quad (2.41)$$

where M_p is the generalised mean amplitude in a specific frequency, n is the number of FRFs and $FRF_i(f)$ is the amplitude of FRF_i in a specific frequency. If $p = 2$ the generalised mean is called the root mean square (RMS). (2.41) can thus be written as

$$RMS(f) = \sqrt{\frac{FRF_1^2(f) + \dots + FRF_n^2(f)}{n}} \quad (2.42)$$

The RMS is calculated for all frequencies in a certain frequency range, and is then denoted RMS FRF.

3. Numerical Pre–Test Analyses

Numerical pre–test analyses were performed to get an indication of what could be expected in the measurements. The knowledge obtained was also used when designing the experimental setup.

The panel was modelled and analysed, both with and without carpet, using the FE method. For the panel without carpet, the eigenfrequencies and mode shapes were computed. Sensor and excitation positions, for the experimental measurements of the panel, were then decided based on these results. Also, both the effect of the sensor masses and the position and stiffness of the rubber bands (used to suspend the test specimens in the experimental measurements), were studied and evaluated.

In the case where the panel model included a carpet, the carpet was modelled using solid elements. FRFs and the overall vibrational response of both panel and heavy layer were computed to determine an upper frequency of interest in the experimental measurements. The upper frequency of interest was well above the frequency where the heavy layer started showing tendencies of being vibration isolated. Additionally, the effect of the accelerometer mass on the heavy layer was studied. The overall response of the surfaces, such as the panel or heavy layer, were evaluated using the Equivalent Radiated Power (ERP).

3.1 Numerical Model of Example Structure

The numerical model was created from CAD drawings provided by Volvo Cars. The CAD drawings were used to create a FE mesh. The mesh was created with the *Batch Mesh* tool in ANSA and had to fulfil the mesh criteria set by Volvo Cars. In order to fulfil the mesh criteria and make as few simplifications of the geometry of the model as possible, the element size used for the panel was $2.5 \times 2.5 \text{ mm}^2$. For the foam the element size was $2.5 \times 2.5 \times 2.5 \text{ mm}^3$, and for the heavy layer it was $2.5 \times 2.5 \times 1 \text{ mm}^3$. For reference, Volvo Cars use a $5.0 \times 5.0 \text{ mm}^2$ mesh in their models for applications alike. No convergence study was therefore performed since it was assumed that the mesh was fine enough, as long as it fulfilled the mesh criteria. It is likely that a rougher mesh could be sufficient enough. However, since the model was quite small, compared to a model of a complete body, it was decided to not optimise the mesh.

To create a FE model from the CAD model, the software ANSA was used. Ansa is a widely used pre-processor developed by Beta CAE Systems. The calculations were performed in MSC Nastran, provided by MSC Software. Depending on what

type of calculation performed in MSC Nastran, different solvers were used. The specific solvers used for the analyses are presented in Table 3.1. All results were post processed and visualised in the post-processor Meta, developed by Beta CAE Systems. Some data was also processed and visualised in Matlab, which is a numerical computing environment developed by MathWorks.

Table 3.1: MSC Nastran solvers used in the analyses.

Solver	Application
103	Eigenvalue problem
111	Frequency response functions
111	Equivalent radiated power

3.1.1 Modelling of Panel

The numerical model of the panel was created with a CAD model as base, as mentioned in Chapter 3.1. The CAD model was trimmed according to the experimental model, presented in Chapter 1.4. The panel was meshed with shell elements according to the criteria used at Volvo Cars. The model is presented in Figure 3.1. The material model used was an isotropic linear-elastic material model with material parameters according to Table 3.2. The material parameters were provided by Volvo Cars.

Table 3.2: Material parameters for the panel.

Material	E [GPa]	ν [-]	ρ [kg/m ³]
Steel	210	0.30	7850

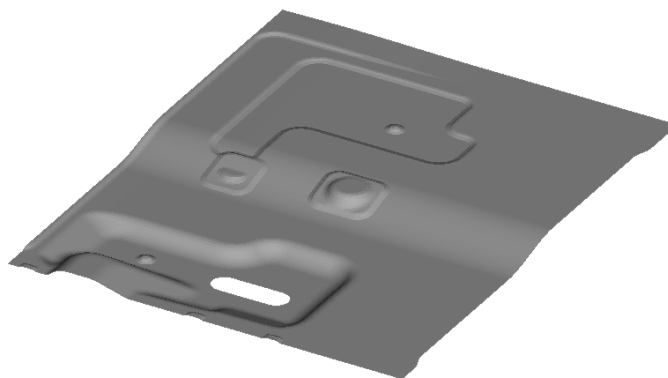


Figure 3.1: Geometry of panel.

3.1.2 Modelling of Carpet

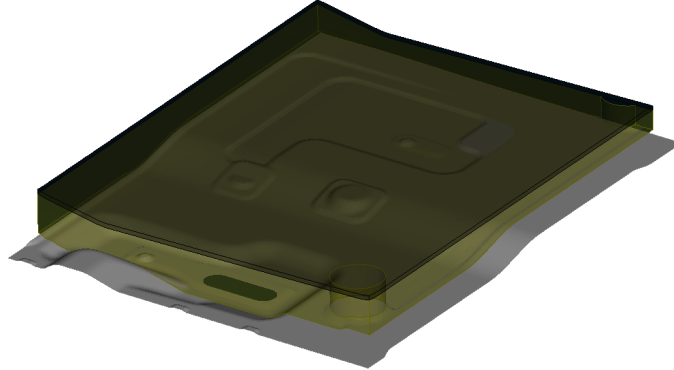


Figure 3.2: Geometry of panel and carpet.

The carpet was modelled with solid elements. The CAD model contained the top and bottom layer of the foam layer of the carpet. The top layer was meshed according to the same criteria as the panel with shell elements, whereon the solid elements was created by using the tool *Extrude* in ANSA. This tool extrudes a solid mesh from the meshed top surface to the bottom surface of the carpet. The heavy layer was then created by adding a solid mesh on top of the foam. The carpet (foam and heavy layer) is presented in Figure 3.2.

The material model that was used was an isotropic linear-elastic material model, both for foam and heavy layer. The material parameters used for the carpet are presented in Table 3.3. The material parameters were provided by Volvo Cars.

Table 3.3: Material parameter for foam and heavy layer.

Material	E [kPa]	ν [-]	ρ [kg/m ³]
Foam	80	0.41	60
Heavy layer	10000	0.40	750

3.1.3 Modelling of Interface

The interface between panel and foam were modelled with RBE3 elements in ANSA. This connection defines a displacement relation between the nodes of the panel mesh and the nodes of the foam surface mesh closest to the panel. The displacements of the nodes of the foam are calculated as a mean value of the closest nodes on the panel.

The CAD model, which was used to create the mesh of panel and carpet, had some overlap between the panel and carpet. The foam of the carpet penetrated the panel in some areas. Since the connection used in the model did not take into account contact between bodies, this was not a problem for the connection conditions. When defining the contact between panel and foam, the condition was to couple every surface node of the foam that were located less than 1 mm from

any of the nodes of the panel. This gave a generally good connection, but there were some areas of foam and panel that were not connected. Figure 3.3 shows which areas that are connected and which areas that are not. The areas where the foam penetrates the panel are marked with red circles.

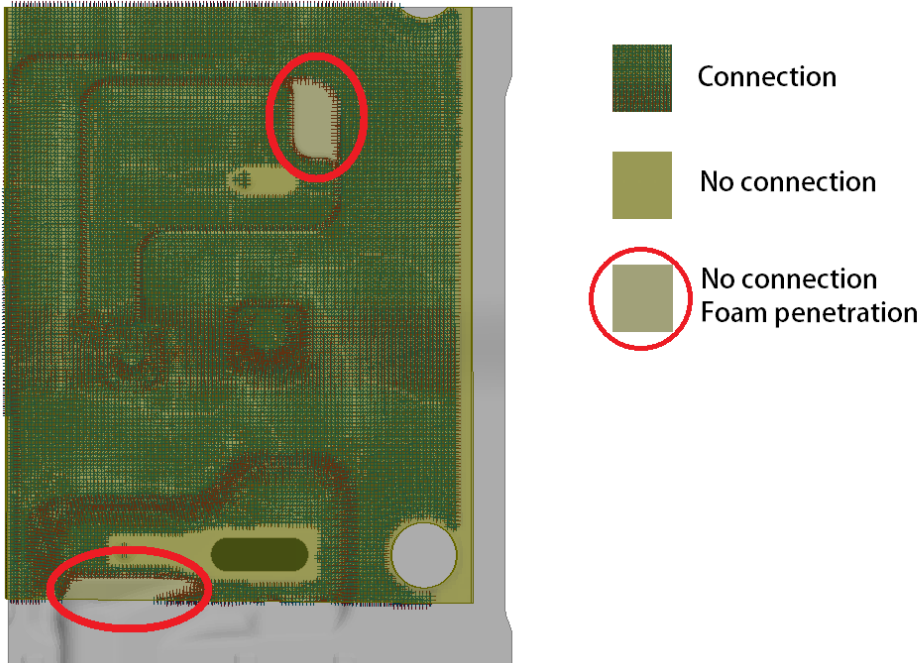


Figure 3.3: Model showing the connected area between panel and foam. The parts of the foam which penetrates the panel are marked.

3.2 Vibrational Response of Panel and Carpet

The dynamic behaviour of the numerical model was studied in order to get an indication of what was to be expected in the experimental measurements. Further, the effect of boundary conditions and accelerometers were studied to get an indication of how the experimental setup would affect the measurements. These studies and results are presented below.

3.2.1 Dynamic Behaviour in Different Frequency Ranges

An objective of the numerical pre-test analyses was to get an indication of the dynamic behaviour of panel and carpet in different frequency ranges. As discussed in Chapter 1.1, current modelling strategy uses NSM to represent the carpet. However, it is believed that an isotropic linear-elastic model would give a better prediction of the behaviour of the panel and carpet. The two modelling strategies was therefore evaluated. The panel was excited by a dynamic unit load from 0 to 1000 Hz. Structural modal damping was used with a loss factor of 0.08 over the whole frequency

range, and the ERP of the panel surface was computed. These results were also used to get an indication of what was to expect in the experimental measurements.

The ERP of the panel with carpet modelled as NSM vs the panel with the carpet modelled with solid elements are presented in Figure 3.4. As expected, the vibrational response differs between the two models. In the frequency range 0–100 Hz, the two curves follow each other quite well. There is a small shift in the peaks, which is assumed to be an effect of the stiffness of the solid carpet representation. However, this effect is small. Above 100 Hz, the behaviour shown by the two curves starts to differ more. From about 100 Hz up to 450 Hz, the panel with the NSM representation of the carpet has higher vibration response level and different resonance peaks compared to the panel with the solid representation of the carpet. Above 450 Hz the panel with the solid representation of the carpet has higher vibration response level.

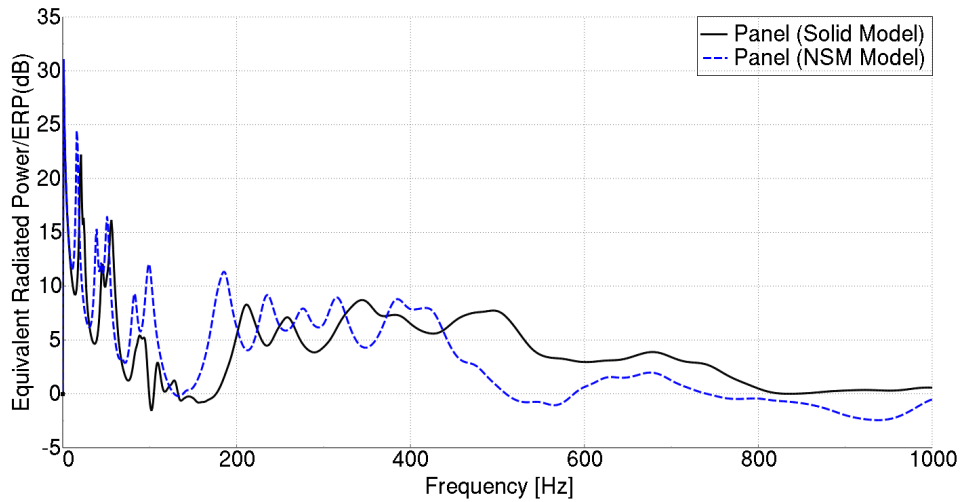


Figure 3.4: The equivalent radiated power of the panel where the carpet is modelled as NSM (Blue line) and where the carpet is modelled with solid elements (Black line).

The ERP of the panel vs the heavy layer, calculated using the model with the solid representation of the carpet, is presented in Figure 3.5. In the low frequency range, 0–100 Hz, the curves follow each other. However, the amplitude of the heavy layer is slightly lower compared to the curve of the panel. This is due to the smaller surface of the heavy layer compared to the panel. Between 100–200 Hz, the vibrational response in the heavy layer is higher than in the panel. Above 200 Hz, the vibrational response in the panel are significantly higher than in the heavy layer.

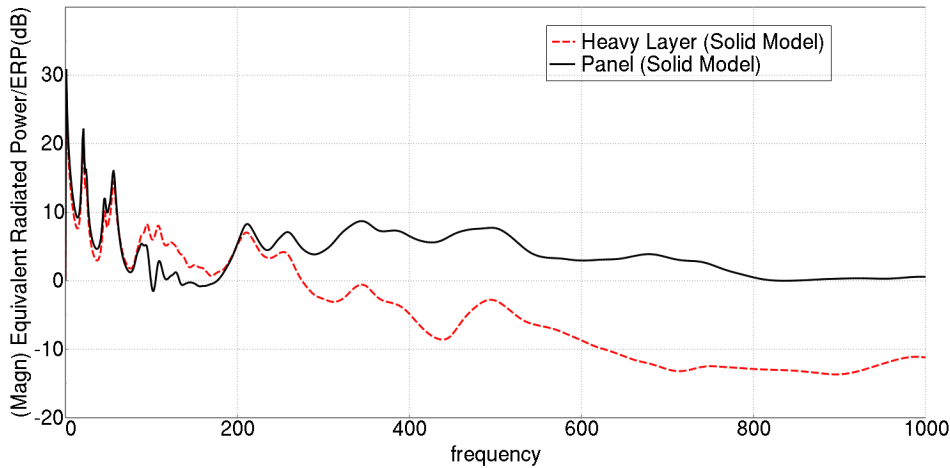


Figure 3.5: The equivalent radiated power of the panel (Black line) vs the heavy layer (Red dashed line) for the model where the carpet is modelled with solid elements.

3.2.2 Influence of Accelerometer Mass

Gluing the accelerometers to the heavy layer were thought to increase the stiffness and mass of the heavy layer locally. Both of these effects were assumed to reduce the response in the point of the measurement.

To get an indication of how much effect the accelerometers could have on the measured FRFs, these were calculated with and without accelerometers in the model. The accelerometer was modelled as a point mass 4 mm above a node on the surface of the heavy layer. The accelerometer was connected to the closest nine nodes on the surface by RBE3 elements. The connection is explained in Chapter 3.1.3. Two points, (1) and (2), were chosen. Point (1) on the panel and point (2) just above on the surface of the heavy layer. A dynamic unit load excited the panel in a third point, (3). The transfer functions for (3) to (1) and, (3) to (2) were calculated. This was done for the same model without and without an accelerometer in point (2). The calculated FRFs are presented in Figure 3.6.

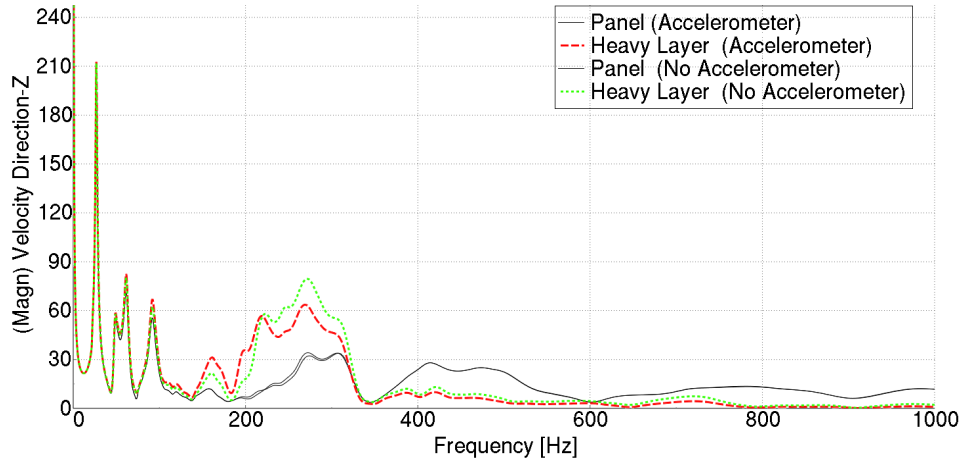


Figure 3.6: Panel and heavy layer FRFs, with and without accelerometer. Black lines show the FRFs of the panel, with and without accelerometer. Green dotted line shows FRF to heavy layer without accelerometer, and red dashed line shows FRF to heavy layer with accelerometer.

There are some interesting observations made from the FRFs presented in Figure 3.6. First, the influence of the accelerometer on the response in the panel is negligible. The two black curves seemingly follows each other perfectly. Secondly, comparing the responses of the heavy layer one can see a clear effect of the accelerometer. In the frequency range 0–150 Hz, the response in the point on the heavy layer is barely affected by the accelerometer. The small affect that can be observed in this frequency range is that the response in the peaks is higher with the accelerometer. However, the effect of the accelerometer in this frequency range is limited.

In the frequency range 150–220 Hz, the tendency seen in the lower frequency range (0–150 Hz) is much clearer. The response in the point on the heavy layer with accelerometer is clearly higher. In the frequency range 220–350 Hz, the response is generally higher without the accelerometer. Above 400 Hz, where the heavy layer becomes vibration isolated, there is only a small impact of the accelerometer, which seems to lower the response in the measuring point.

The conclusion from these results is that the accelerometer is likely to have an influence on the measurements. However, the difference in amplitude of the response of the panel and heavy layer is large enough to see a difference in their responses. Therefore, the influence of the accelerometer should not influence the measurements in such a way that the behaviour of the panel and heavy layer can not be determined with a reasonably good precision. More specifically, tendencies of the expected behaviour should be observable in the measurements regardless of the accelerometer.

3.2.3 Influence of Boundary Conditions

The effect of two different boundary conditions, on the eigenfrequencies and FRFs, were evaluated. In both cases, the boundary conditions mimic horizontal suspension

of the panel to allow the carpets to be placed on top. The suspension should also be stiff enough to prevent the carpets from falling off or moving due to excitations. The panels were to be suspended in four points and two alternatives were investigated. The connection points of the boundary conditions were placed either in the corners or in the midpoints of the boundaries. The suspension was modelled by connecting spring elements between the chosen points and fixed points above these. The stiffness of the springs was decided by assuming the suspended panel behaved as a spring-mass system. The combined spring stiffness was then chosen so that the first eigenfrequency of the spring-mass system would be 2 Hz. This value was chosen since this was the aim in the experimental setup, see Chapter 4.1 for further explanation.

It was concluded that both alternatives had a little effect on the eigenfrequencies of the panel. However, the alternative where the panel was suspended in the midpoints of the boundaries affected the eigenfrequencies the least. This was therefore the alternative used in the experimental measurements.

3.3 Frequency Response Function vs Equivalent Radiated Power

It was not possible to measure the response in enough points to calculate the ERP in a reliable manner in the experimental measurements. The response was measured in four points on the panel and four points on the heavy layer. The RMS was then calculated from the four FRFs of each surface. This is explained in more detail in Chapter 4. The objective of the pre-analysis explained here was to determine how good of a predictor the RMS FRFs are for the ERP of the whole surface.

Figure 3.7 and 3.8 presents a comparison between the RMS FRFs and the ERP of two surfaces. Each figure presents two RMS FRFs and two ERP curves. One RMS FRF describes the combined response of the four points on the panel. The other RMS FRF describes the response of the four points on the heavy layer. The ERP curves describes the overall response, one of the panel and one of the heavy layer. The responses presented the figures are calculated in the same points, but for different excitation points. The location of the response and excitation points are the same as was used in the experimental measurements. See Chapter 4 for further details.

Since RMS FRFs and ERP curves are different measurements, one should be cautious comparing them. In addition, the RMS FRF is based on measurements in very few points compared to the ERP. It is therefore not the goal to capture the exact behaviour of the surface, but to see if tendencies of the behaviour, displayed by the ERP measurement, can be observed by just measuring the response in a few points.

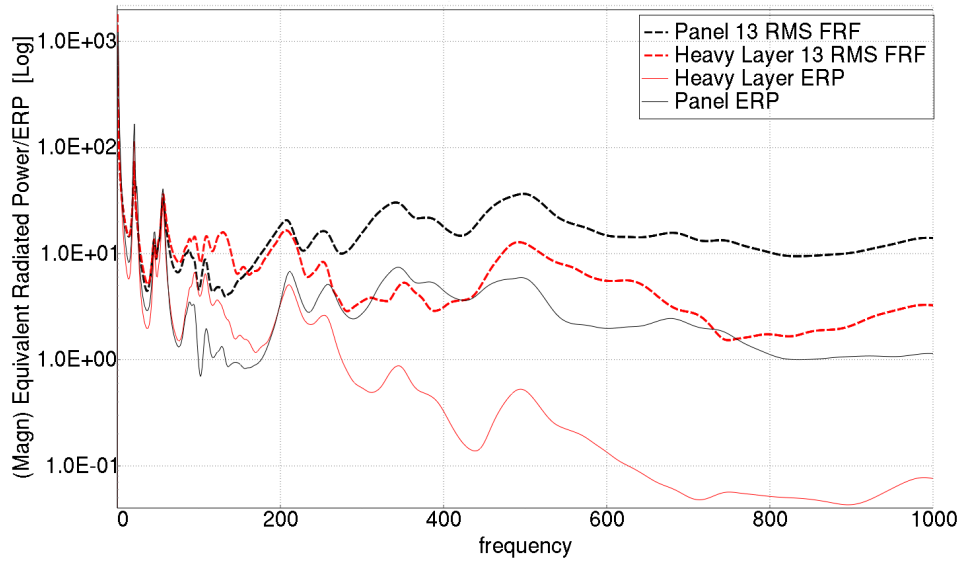


Figure 3.7: ERP of panel (black) and heavy layer (red) vs RMS FRF of the panel (dashed black) and heavy layer (dashed red).

In Figure 3.7, one can observe similar tendencies between the RMS FRFs and the ERP curves. In the frequency range 0-80 Hz, both the RMS FRFs and ERP curves display an added mass behaviour. That is, the curves of heavy layer and panel follows each other. The frequency range where the response in the heavy layer is higher than the response in the panel, is similar between the two measures. The RMS FRFs display a resonant behaviour of the heavy layer in the frequency range 80–160 Hz, while the ERP curves display the same behaviour in the frequency range 80-190 Hz. In the frequency range above 160 Hz for the RMS FRFs, and above 190 Hz for the ERP curves, both measures show clear tendencies of the heavy layer being vibration isolated.

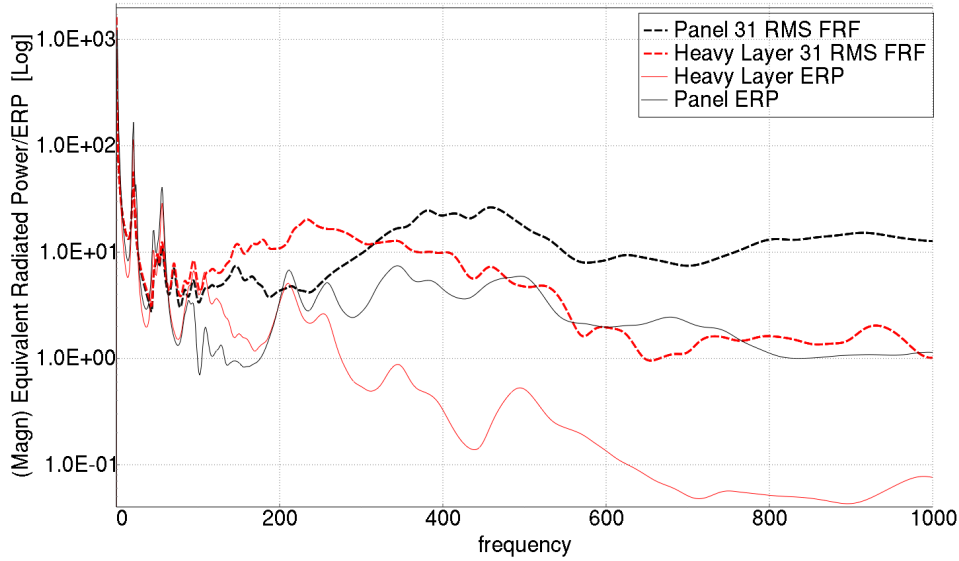


Figure 3.8: ERP of panel (black) and heavy layer (red) against RMS FRF of the panel (dashed black) and heavy layer (dashed red).

The tendencies displayed by the RMS FRFs and the ERP curves in Figure 3.8, do not share their characteristics as well as they do in Figure 3.7. In the frequency range 0–80 Hz, both RMS FRFs and ERP curve display the same tendencies of an added mass behaviour. However, the frequency range where tendencies of a resonant behaviour of the heavy layer can be observed differs between the two measurements. The RMS FRFs displays a behaviour where the response of the heavy layer is higher than the response in the panel in the frequency range 80–310 Hz. The ERP curves show the same behaviour in the frequency range 80–160 Hz, as stated earlier. Both measurements shows clear tendencies of a vibration isolated heavy layer in frequencies above the resonant behaviour of the heavy layer.

The conclusion to draw from the data presented in Figure 3.7 and 3.8 is that the RMS FRFs show clear tendencies of the expected behaviour. However, the behaviour displayed by the RMS FRFs should not be seen as representation of the response of the surfaces, but as a measure that indicates a the behaviour of the surfaces in a frequency range. One should also be aware of that the frequency range, in which, tendencies of a specific behaviour is observed have a variance dependent on the excitation point.

4. Experimental Analysis

This chapter treats the experimental analysis. To be more specific, this chapter includes, general information about the measurements and the test specimen, measurement methodology, results from the measurement, and a discussion of these.

The example structure which the measurements were performed on is presented in Chapter 1.4. There were five sets of the example structure, i.e. five panels and five carpets, available. The measurements are divided into two series. The objective of the first series was to increase the knowledge of the dynamic behaviour of panels. This included a study of the effect of carpets and the contact condition of these on the dynamic behaviour of a panel. It also included a dispersion study of five panel specimen. In the second series, the objective was to evaluate the dynamic response of panel and heavy layer relative to each other. The effect of contact conditions were also evaluate.

Before the two measurement series were performed, the experimental setup was validated. It is important that the free-free suspension does not interfere with the measurements. The resonance frequencies of the rigid body modes should be well below the resonance frequency of the first flexible mode. It is also important that the suspension does not add too much damping to the structure. The repeatability of the measurements were also validated by performing a number of measurement were one parameter were change at the time.

4.1 Experimental Setup

The specimen were suspended horizontally, using light rubber bands to emulate free-free conditions. The setup is presented in Figure 4.1. The free-free suspension essentially means that there are no boundary conditions, that the test subject should be floating in space. Since these conditions are not possible to produce in a real physical measurement, approximations have to be made.

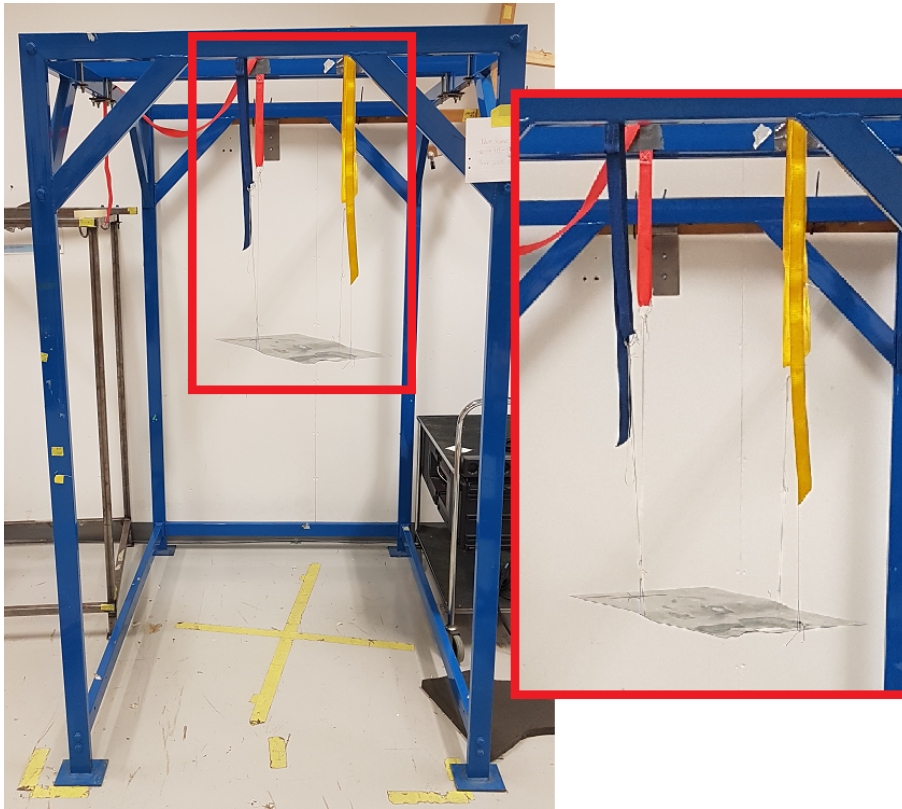


Figure 4.1: The rack which the test specimen were suspended from.

Free-free conditions are often used in model validation, and the fact that the free-free conditions have to be approximated have contributed to a number of papers dedicated to quantify or describe the effects of these approximations [8] [9] [10]. The authors, mutually, stress the importance of rigid body modes with significant lower resonance frequencies than the resonance frequency of the first flexible mode. A setup which allows a factor 10 between the resonance frequencies seems to be sufficient for most applications. The rigid body modes should then appear no higher than at 2 Hz to not interfere with the flexible modes, since the results presented in Chapter 3.1.2 indicate that the resonance frequency of the first flexible mode is about 20 Hz. This requires rubber bands with a low stiffness.

The resonance frequencies of the rigid body modes could be determined approximately by exciting these modes by hitting the panel. The oscillations of the rigid body modes of the panel were then timed, which gave an approximation of the modes resonance frequencies. This indicated that the resonance frequencies of the rigid body modes and the stiffness of the rubber bands was low enough to not interfere with the flexible modes. The resonance frequencies were later determined more precise in the measurements.

The rubber band were attached to the panels by non-elastic threads. The non-elastic threads were threaded through 1 mm holes, that were drilled in the panels. It was decided to drill holes in the panels and not use glue, since glue could add additional mass and stiffness to the panels. The influence of the holes on the be-

haviour of the panels were assumed to be negligible. The rubber bands were then attached to the rig by straps and cable ties, see Figure 4.2.

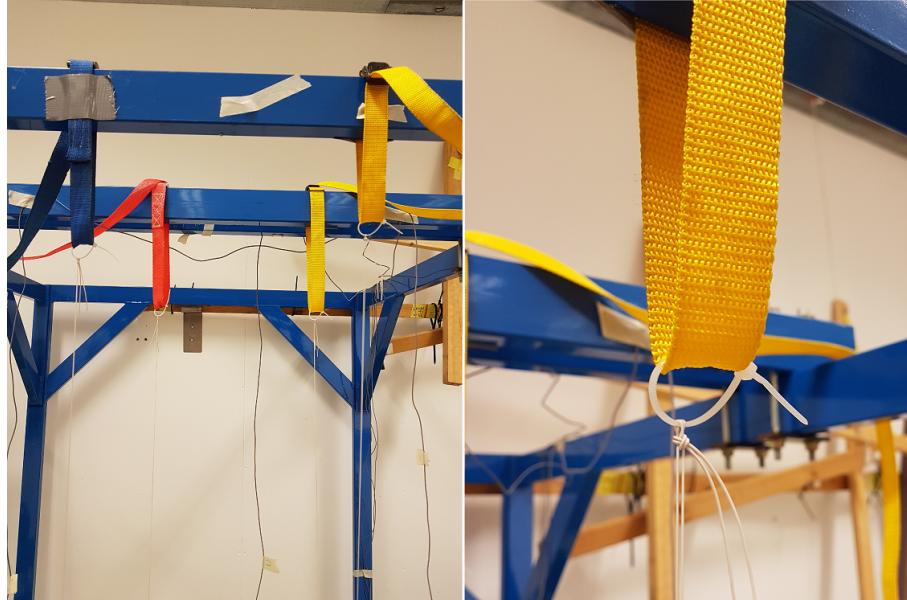


Figure 4.2: Strap-Rig-Rubber band attachment (Left) and a closeup of Strap-Rubber band attachment (Right).

The setup used in the measurements of the panels with carpets was the same setup used in the panel measurements but with some modifications. Since the weight of the panel with a carpet was approximately twice the weight of just the panel, the stiffness of the rubber bands was increased. This was achieved by using twice the amount of rubber bands. To be able to use the same type of suspension as for the panels, with non-elastic thread between the panel and rubber bands, small cuts were made in the carpet. This allowed the non-elastic thread to pass through the carpet. The cuts were assumed to have a negligible affect on the behaviour of the panel-carpet system.

Two hammers were used in the measurements to excite the panels. For the measurements of panels without carpets a PCB Piezotronics 086D80 Miniature Instrumented Impulse Hammer was used. For the measurements of panels with carpets a modified Dytran 5800B5 Impulse Hammer was used. Both hammers are shown in Figure 4.3. The reason for using different hammers in the measurements was that the properties of the test subject required different force levels in the excitations to obtain measurement data with sufficient quality.

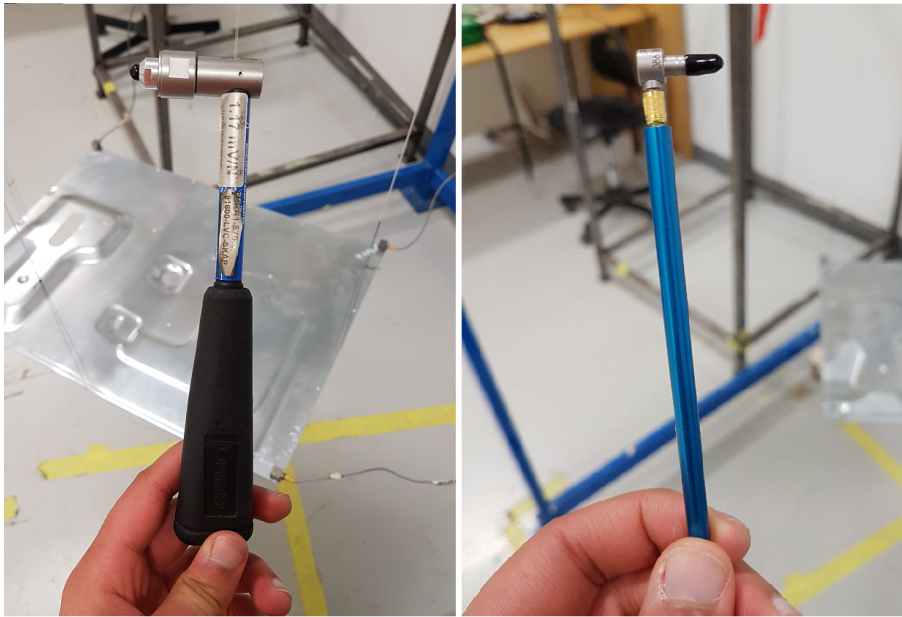


Figure 4.3: Modified Dytran 5800B5 Impulse Hammer (Left) and PCB PIEZOTRONICS 086D80 Miniature Instrumented Impulse Hammer (Right).

The accelerometers used were of type Dytran 3032A Miniature Accelerometer, shown in Figure 4.4. The low weight of 1.5 grams and its slender cable allowed for small interference with the test specimen.

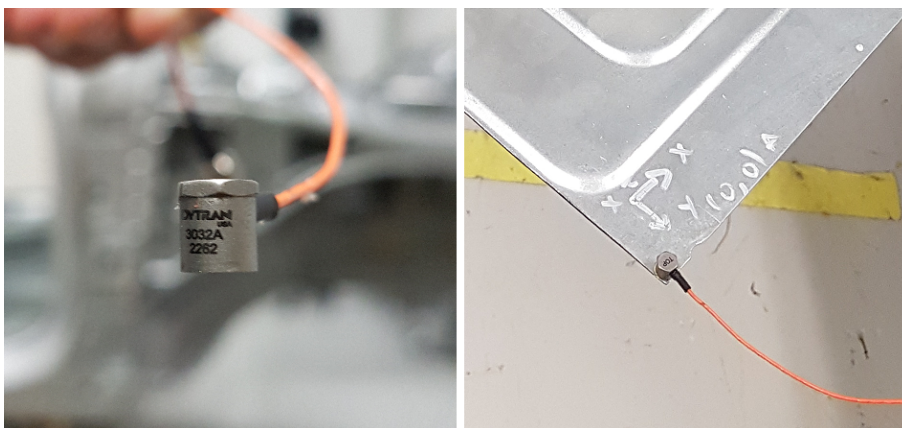


Figure 4.4: Dytran 3032A Miniature Accelerometer

4.2 Measurement Errors and Measurement Procedure

To ensure that a measurement is reliable, considerations to potential errors have to be made. Errors are usually divided into systematic and random errors. Systematic errors are errors that are not caused by chance but are predictable. These will have

no impact on the repeatability of the measurements, and are therefore harder to detect. Random errors are errors that are unpredictable and will have a negative impact on the repeatability of a measurement. For instance, if a constant quantity is measured multiple times, the measured values will vary due to random errors. To minimise the risk for errors in the measurements, the measurements were performed according to a given procedure. The influence of experimental setup was also evaluated.

4.2.1 Measurement Procedure

The following part describes how the measurements were conducted. They were conducted in this manner to reduce the risk of poor repeatability, i.e. to reduce the risk, or the impact, of random errors.

When measuring a FRF, a point in the panel is excited by a hammer strike and the vibrational response is measured in another point. Since the hammer is hand held, there is a variation of precision between the excitations. Therefore, an average of five FRFs is calculated for each FRF. In practice this means that the panel is excited five times in the same spot and the response is measured for each of the excitations. The average is then calculated from these five excitations. By averaging, the effect of the variations of the excitation is reduced.

Each excitation needed to fulfil a number of criteria to be considered valid. Otherwise they were excluded. The purpose of this was to reduce the risk of random errors. The first criteria handled the precision of the excitation. All hammer strikes that appeared to have hit further away from the intended excitation point than 5 mm were directly excluded. Other criteria the excitation also needed to fulfil were a force criteria, a frequency content linearity criteria and a coherence criteria. The force criteria was set so that noise should have a minimal impact in the measured FRFs. This meant in practice that a certain amount of force needed to be generated by the hammer strike. The frequency content linearity criteria ensured that no frequencies across the frequency range of interest were not excited with enough force to get a high enough response. In the cases where this criteria could not be fulfilled, the coherence suffered in the frequency range which was not excited properly. The coherence criteria was quite arbitrary since the coherence depended on the excitation and response point chosen. Instead of a strict criteria a rule of thumb and judgement was used. If the coherence changed more than what was assessed plausible the measure was excluded. The force and frequency content of the excitation and the coherence of the FRF were all registered or calculated and shown instantaneously after the excitation was performed by the software.

4.2.2 Effect of Experimental Setup Parameters on Measured Behaviour

The repeatability of the measurements depends on the experimental setup and on how the measurements are performed. The experimental setup and the measurement equipment should not interfere with the behaviour of the specimen. If they do, the

effect must be known and compensated for. Otherwise the measurements cannot be used. Parameters that were believed to might interfere with the behaviour of the specimen were therefore isolated and investigated. In order to evaluate whether they interfered with the behaviour of the specimen or not.

Reference FRF

Although, the criteria discussed in Chapter 4.2.1 improved the conditions for repeatability they do not take the sensitivity of variation of excitation point into account. Since the coherence is calculated using the first FRF as reference it is possible that if the panel is sensitive to small variation in the point excitation, an excitation that fulfils the criteria above may not give the same response as a seemingly identical excitation. To determine the sensitivity to small variations of position of excitation five averages of FRFs were compared to each other. The FRFs obtained from the measurements compared with the average FRF from another panel showed that the influence of small variations of the impact are small compared to the variation between the two panels.

Small Variation of Accelerometer Position

Since a maximum of two accelerometers were used in the measurements, the accelerometers needed to be moved between the measurements on each panel and carpet. Moving the accelerometers had two effects on the measurements. First, the mass of the accelerometers will change the mass distribution of the panel and carpet and secondly, the position of the accelerometer may vary slightly from panel to panel and heavy layer to heavy layer. In order to determine how much of an impact a slight variation in accelerometer position had, measurements were performed on a panel where the accelerometer position varied between the measurements. The positions chosen were approximately ± 5 mm in the x- and y-direction apart, which was assessed to be a much larger variation of position than what could be expected in the measurements. A picture of the placement of the accelerometer can be seen in Figure A.1 in Appendix A. The FRFs obtained from these measurements compared with the FRF from another panel are presented in Figure 4.5. The figure shows that the position of accelerometer had a small impact on the FRF compared to the variation between the panels.

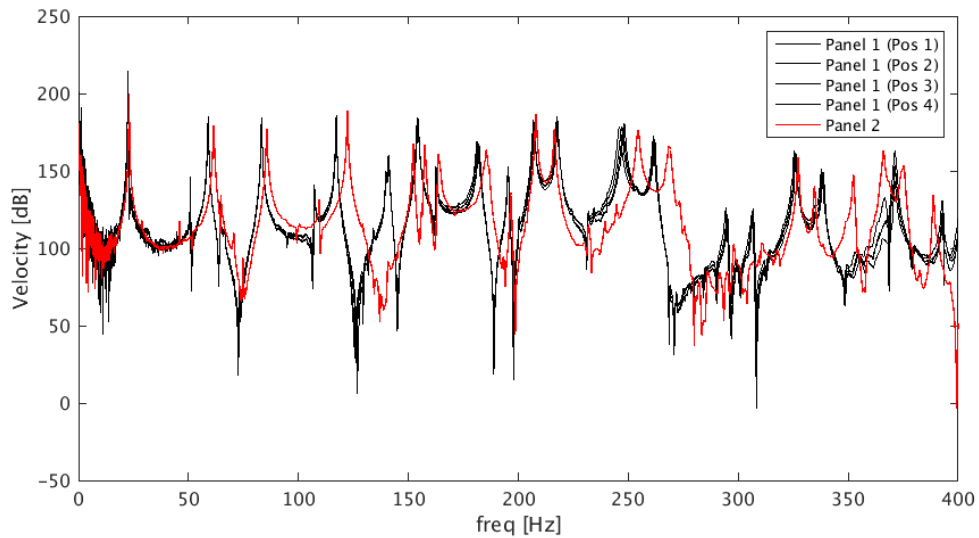


Figure 4.5: FRFs for Panel 1 (Black lines) vs FRF for Panel 2.

Large Variation of Accelerometer

To determine the effect of moving the accelerometer to another part of the panel, three measurements were made. The accelerometer was placed in one of three corners of the panel for each measurement. The panel was excited in the same point for each measurement. Since the compared FRF are not the same FRF only the resonance frequencies can be compared between the FRFs. One problem with this approach is that a thought variation in resonance frequencies of a mode could be two different modes with a small difference in frequency. One mode showing in one FRF and another mode showing in the other FRF. To rule this out, the calculated eigenfrequencies was used to assure that there only were one mode present around that certain frequency. The comparison between the three measured FRF are presented in Figure 4.6. It can be noticed that resonance frequencies are influenced by the accelerometer. However, the influence of the accelerometers on the resonance frequencies are small compared to the variation between the panels.

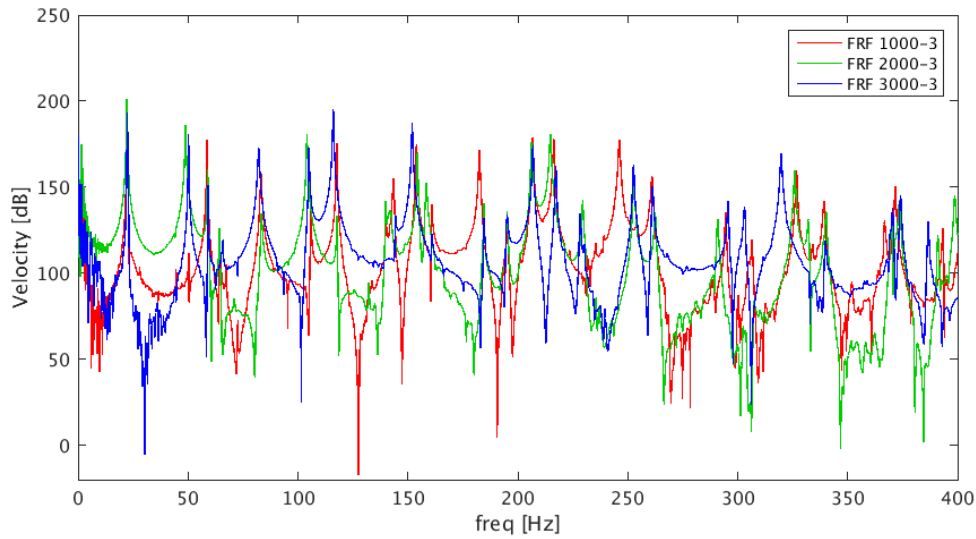


Figure 4.6: FRFs for Panel 1. The FRF are measured in different positions

Cable Position

There were indications that the mass and stiffness of the accelerometer cable could influence the behaviour of the panel. In order to determine the impact of variations in how the cables were suspended, five different positions and lengths of the cable were studied. The different cable suspensions are presented in Figure A.2 in Appendix A. The measured FRFs compared to the FRF of a different panel are presented in Figure 4.7. It can be concluded that the impact of variation of the cable suspensions are small compared to the variation between panels. However, the FRFs indicated that a more tensed cable, D) in Figure A.2 in Appendix A, seemed to increase the damping in the panel.

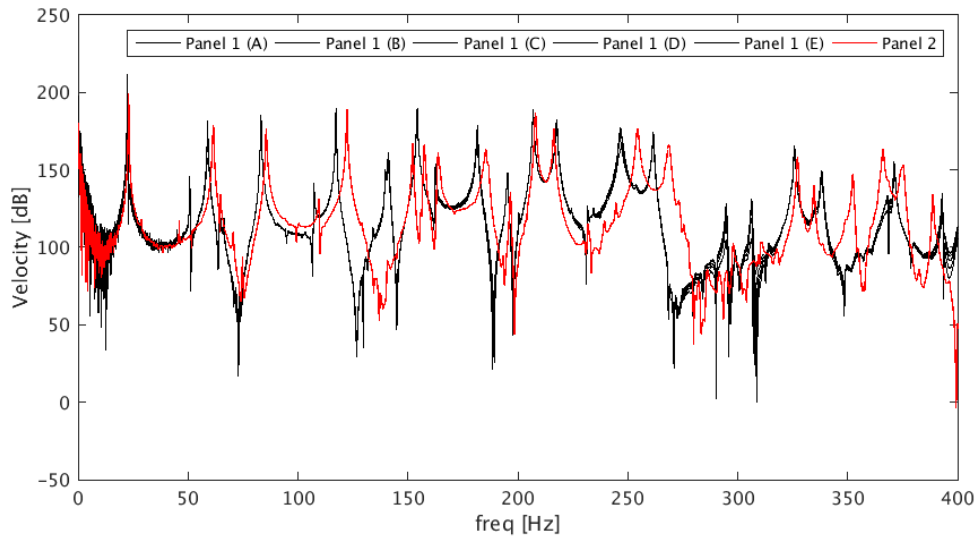


Figure 4.7: FRFs for Panel 1 with five different cable positions (black) vs the same FRF for Panel 2 (red).

Length of Non-Elastic Thread

It was also of interest to study how the measurements were affected by changing the panel between measurements. Since the non-elastic thread connecting the panels to the rubber bands were change between the measurements of the different panels, it was a concern that this would influence the measurements. Four combinations of threads with different lengths, presented in Figure A.3 in Appendix A, were considered in these measurements. The FRFs obtained compared with the FRF of another panel are presented in Figure 4.8. It is clear that the influence of the non-elastic thread is small compared to the variation between the panels.

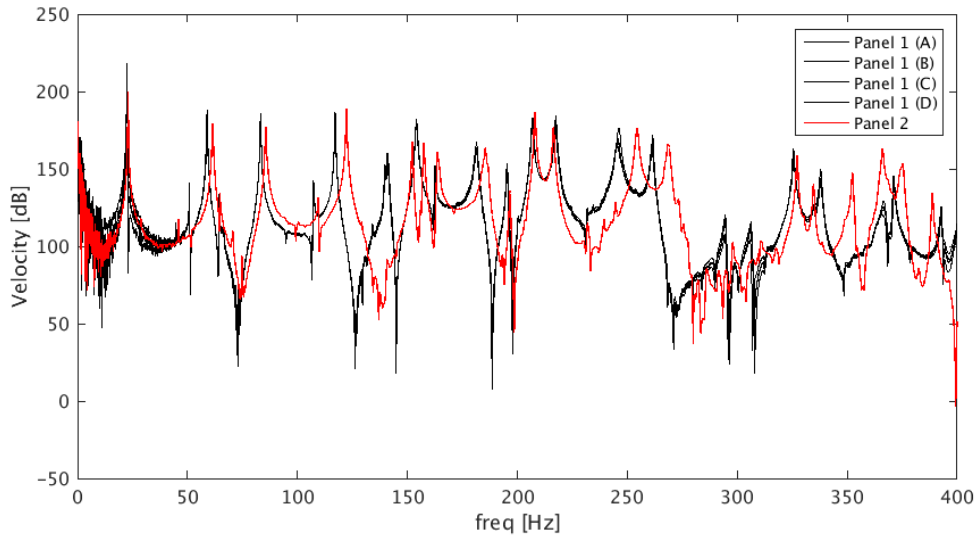


Figure 4.8: FRFs for Panel 1 with five different thread length (black) vs the same FRF for Panel 2 (red).

4.3 Measured Response Functions

The aim of the experimental measurements were to increase the knowledge regarding the dynamic behaviour of panel and heavy layer in the frequency ranges of interest. This was done by measuring response functions for the panel and heavy layer. The response of the panels and heavy layers were measured in a number of points. It was of interest to evaluate the dynamic behaviour and determine if the expected behaviour, mentioned in Chapter 1.1, was present in the measurements. It was also of interest to study how sensitive the dynamic behaviour of the panels and heavy layer was to different contact conditions and arbitrary variations in these. Before any of these measurements were performed, dispersion measurements of the five panels were performed. Two panels were then chosen for the remaining measurements. The chosen panels were Panel 1 and 5. The following part describes the measurements on the two chosen panels.

The measurements on Panel 1 and 5 also included five carpets. The first of these measurements were the response measurements of panel 1 and 5 without carpets. One carpet was then glued to panel 1. Panel 5 had no carpets glued to it, but carpets solely laid on top of it. For the panels with carpets, the response was measured on both panel and heavy layer of the carpet. Since panel 1 had a carpet glued to it, it was not possible to change carpet. Panel 5 had no carpets glued to it. It was therefore possible to change carpet. Thus, the measurements on panel 5 included four carpets. A summary of the measurements are presented below.

Following responses were measured:

- Dynamic response of panel without carpet.
- Dynamic response of panel with glued carpet.
- Dynamic response of panel with non-glued carpets.
- Dynamic response of heavy layer of glued carpet.
- Dynamic response of heavy layer of non-glued carpets.

The vibrational response was measured in multiple points, on both panel and heavy layer. For every point on the panel, there were a point just above on the heavy layer. Figure 4.9 shows the location of the points. As mentioned in Chapter 2.4.2, the RMS of a number of FRFs was used as a measurement of the general response of a surface. The RMS of a number of FRF are hereinafter referred to as a RMS FRF. The RMS FRFs is often followed by a number, that specifies which point on the panel that were excited. An example is the RMS FRF 13 heavy layer. Here the panel is excited in point 13 and the response is measured in point 11, 13, 31 and 33 on the heavy layer. The RMS FRF of the four FRFs obtained in the measurement, is then called RMS FRF 13 heavy layer. If the panel was excited in point 31 instead. The calculated RMS FRF would be called RMS FRF 31 heavy layer. Further, if the response is measured in the same four points on the panel instead of the heavy layer, the RMS FRF would be referred to as RMS FRF 31 panel.

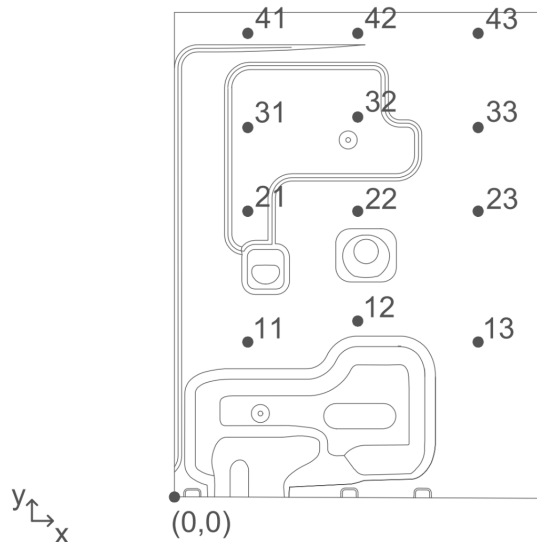


Figure 4.9: Drawing of the panel showing the points where the response was measured in the measurements of Panel 1 and 5 with and without carpets.

4.3.1 Dispersion Study

Measurements to investigate the dispersion of the dynamic behaviour of the five panels were performed. The dynamic behaviour of the panels was evaluated in the frequency range 0–200 Hz. The mode shapes calculated in the pilot studies indicated that to be able to measure the response of all modes up to 200 Hz, the response in at least two points on had to be measured. However, it was decided to measure the response in three points. To not interfere with the behaviour of the panels more than necessary, only one accelerometer was used in these measurements. This meant that the accelerometer had to be moved between the measuring point. For each of the accelerometer positions point 1, 2 and 3 were excited. The excitation points were decided by analysing the modal shapes obtained in the pilot studies. The three points were together assessed to excite all modes up to 200 Hz. Three FRFs per accelerometer position was obtained, nine in total. The corresponding FRF of each panel were then compared to evaluate the dispersion. Accelerometer positions and excitation points are presented in Figure 4.10.

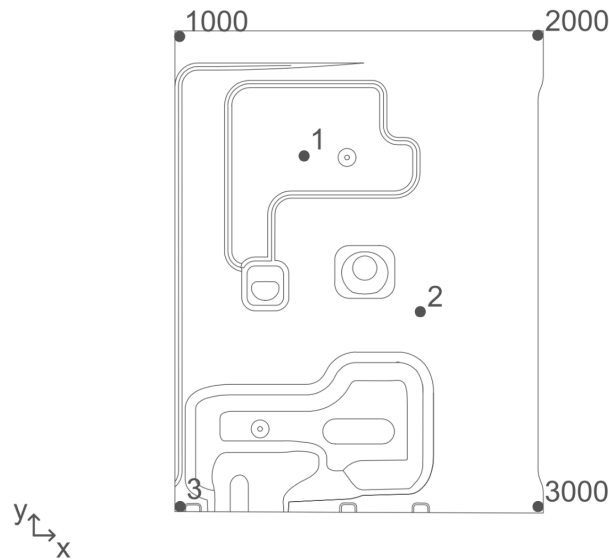


Figure 4.10: Drawing of the panel showing the accelerometer positions (1000, 2000 and 3000) and the excitation positions (1, 2 and 3).

4.3.2 Panel Without Carpet

The measurements of the dynamic response of Panel 1 and Panel 5 without carpets, are described below. The measurements described just below were performed on both panels in the same manner. However, only the measurements of one panel is described.

Panel 1 and Panel 5 measurements

The panel were excited in points 11, 13, 31 and 33, shown in Figure 4.9, and the responses of these excitations were measured in point 13. The four FRFs obtained

from these measurements where composed into a RMS FRF, hereinafter referred to as RMS FRF 13 Panel. The same points were then excited, but the responses were measured in point 31. The four FRFs obtained from these measurements where also composed into a RMS FRF, hereinafter referred to as RMS FRF 31 Panel. Note that this was done fore both panels.

Additional Panel 1 measurements

The measurements described here were only performed on Panel 1. Panel 1 was excited in all points except for point 12, where the responses were measured. Thus, 11 FRFs were obtained from these measurements. The RMS was calculated of these 11 FRFs, generating one RMS FRF, hereinafter referred to as RMS FRF 12 Panel 1. Note that these measurements only were performed on Panel 1.

4.3.3 Panel With Carpet

The measurements of the dynamic response of Panel 1 with a glued carpet were performed in the same manner as for the measurements in the additional measurements without carpet. That is, an accelerometer was placed in point 12 and the panel was excited in the other 11 points.

As stated beginning of the chapter, there were five carpets in total. One of the carpets was glued to Panel 1. The other four carpets were placed, one by one, on Panel 5. Measurements were performed for each of the panel-carpet combinations in the same manner as for the measurements of Panel 5 without carpet. That is, each of the four carpets were placed, one by one, on the suspended panel. The response of the panel were then measured in point 13 and 31 for excitations in points 11, 13, 31 and 33. Two RMS FRFs were calculated for each of the panel-carpet combinations. The experimental setup used in the measurements for both Panel 1 and 5 is shown in Figure 4.11.



Figure 4.11: Panel and carpet with accelerometer.

4.3.4 Heavy Layer

The dynamic response of the heavy layer of the carpet glued to Panel 1, were measured in four points. The points were positioned directly above point 11, 13, 31

and 33 of the panel. The panel were then excited in point 13 and 31. Two RMS FRFs were than calculated. One for the FRFs measured for an excitation in point 13 and one for the FRFs measured for an excitation in point 31. The measurement setup with accelerometers is presented in Figure 4.12.

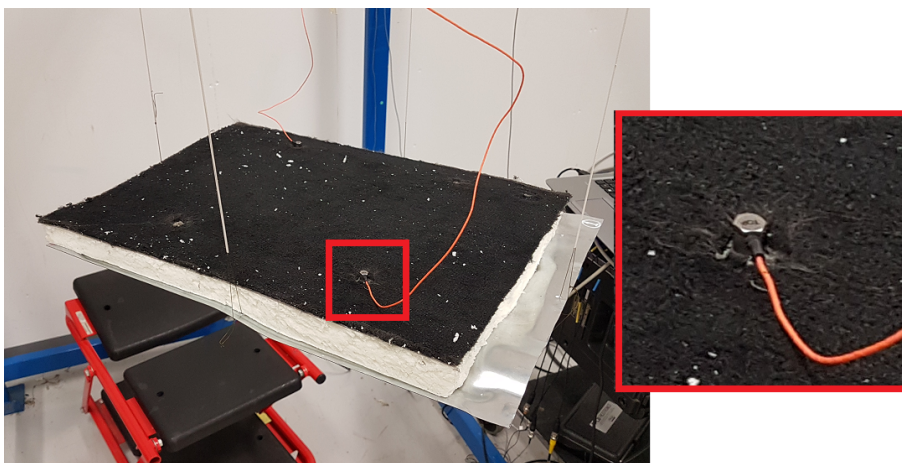


Figure 4.12: Panel with carpet with accelerometers placed in point 13 and 31 on the heavy layer.

The dynamic response of the heavy layers of the non-glued carpets were measured in the same fashion as the dynamic response of the heavy layer of the glued carpet. The dynamic response was measured on each of the four carpets and RMS FRFs were calculated for each of the carpets and excitation point.

4.4 Experimental Results

A large amount of data were acquired during the measurements. Hence, a selection of the data to be presented was necessary. The results of the measurements that were most relevant are presented below.

4.4.1 Effect of Carpet on Panel Response

The results from the measurements on Panel 1 and 5 with and without carpet are presented in Figure 4.13 and 4.14. Note that Panel 1 has a glued carpet, while Panel 5 has non-glued carpets. The result of Panel 5 is the average of the four different carpets tested. Observing both Figures, it is clear that adding carpets to the panels results in a much more damped response. Observe that the response is not measured in the same points for Panel 1 and Panel 5, which calls for caution when comparing the two results to each other. However, it is reasonable to assume that the behaviour seen in these two Figures are representative for the for the whole panel. This would make a comparison between the two applicable. With this said, comparing the effect of adding a carpets to Panel 1 and 5 one can observe a clear difference. The non-glued carpets seems to affect Panel 5 as one can expect. The

first resonance frequency is lowered and the response in the peaks are lower. These effects are probably due to increased mass and damping. The glued carpets affect on Panel 1 is different. Adding a glued carpet seems to shift the whole response curve down, and not only reduce the height of the resonance peaks. One can also observe that the first resonance frequency is higher with the glued carpet than without. This is the opposite as for the panel with non-glued panel, where the first resonance frequency is lower.

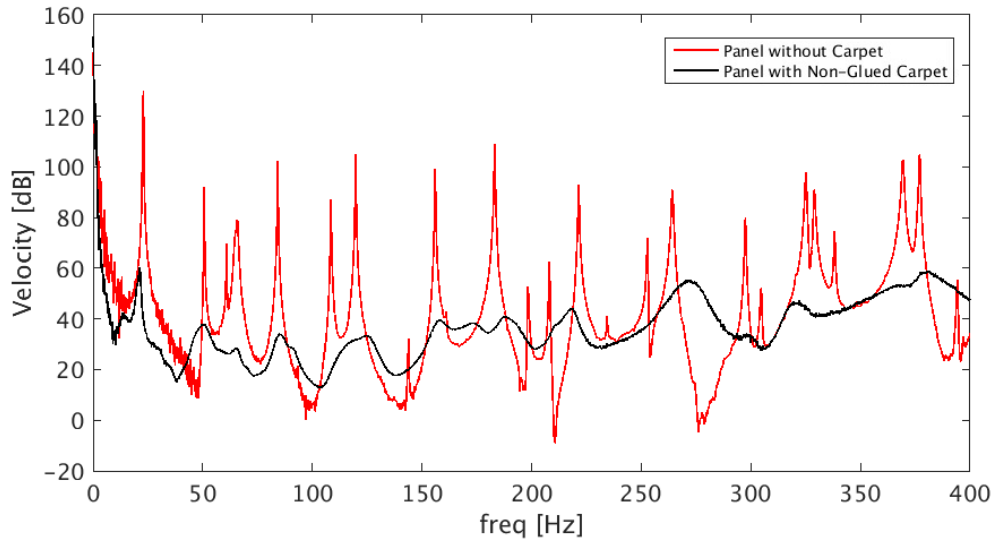


Figure 4.13: RMS FRF 31 for Panel 5 with (Black line) and without (Red line) non-glued carpet.

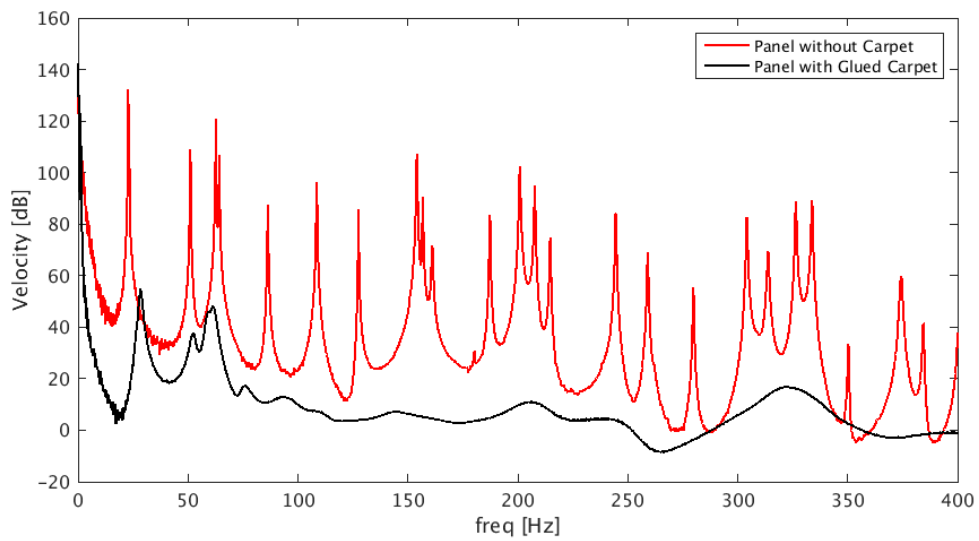


Figure 4.14: RMS FRF 12 for Panel 5 with (Black line) and without (Red line) glued carpet.

4.4.2 Panel vs Heavy Layer Response

Figure 4.15 shows the RMS FRF for Panel 1 and for the heavy layer of the glued carpet. Figure 4.16 shows the RMS FRF for Panel 5 and the mean of the RMS FRFs for the heavy layers of the non-glued carpets. In both cases an excitation in point 13 of the panel is used.

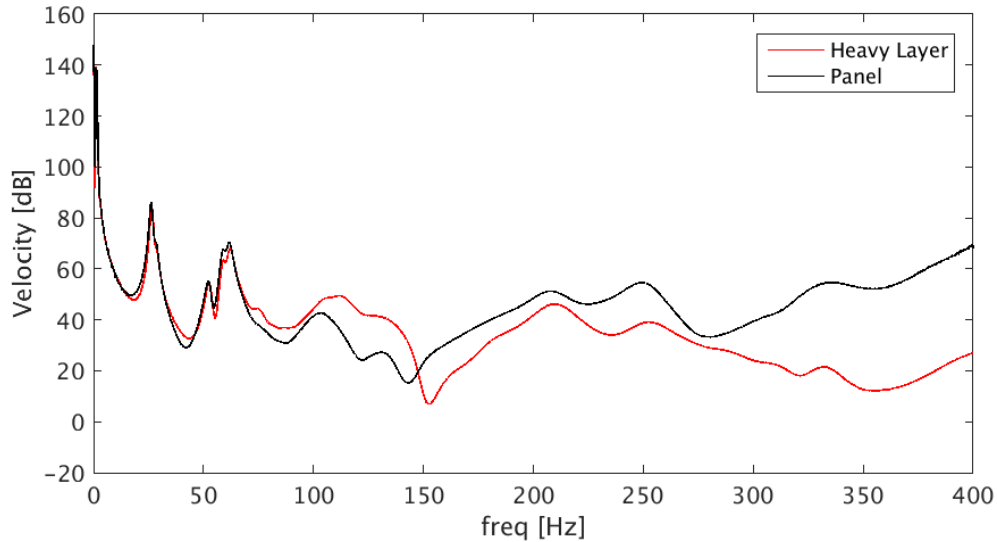


Figure 4.15: RMS FRF 13 for Panel 1 (black line) and RMS FRF 13 of the heavy layer of the glued carpet (red line).

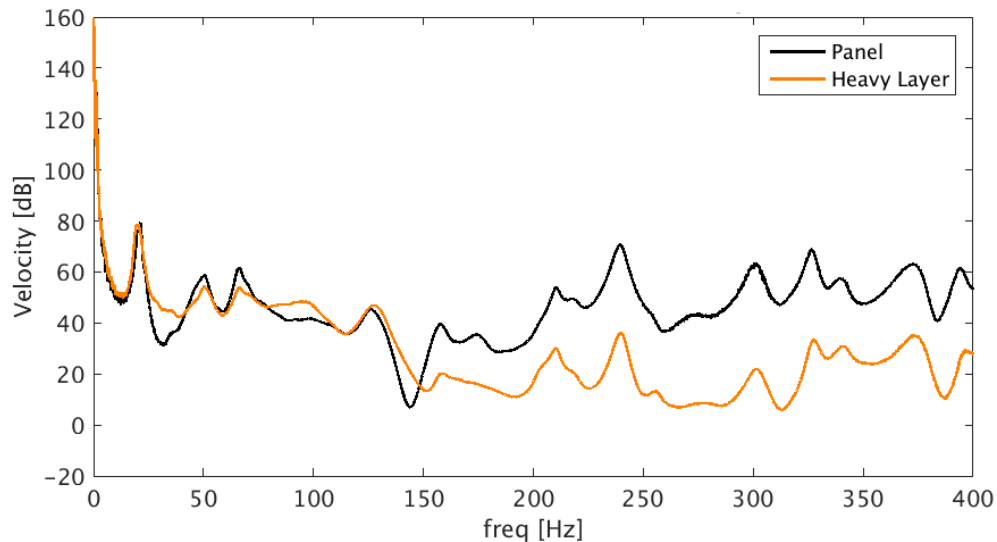


Figure 4.16: RMS FRF 13 for Panel 5 (black line) and the mean of the RMS FRF 13 of the heavy layers of the non-glued carpets (orange line).

In the frequency range 0–75 Hz, the curves of the panel and heavy layer follows

each other in Figure 4.15. This is a strong indication of the pure mass behaviour that was expected. Observing the same frequency range in Figure 4.16, the curves do not follow each other to the same extent. Instead, it seems as the response in the carpet is more damped than the response in the panel. In the frequency range 75–150 Hz, the heavy layer of the glued carpet shows clear tendencies of a resonant behaviour. This behaviour is not as prominent as for the heavy layer of the glued carpet.

The heavy layers of the glued carpet as well as the non-glued carpets show tendencies of being vibration isolated above 150 Hz. However, the difference in amplitude between panel and heavy layer is generally higher in the case with non-glued carpets than with glued carpet.

The characteristics of the response in panels and heavy layers differs depending on glued or non-glued carpet. The smoother RMS FRFs of the setup with glued carpet indicates a more damped system.

4.4.3 Effect of Variations in Carpets

The RMS FRFs for excitation in point 13 of Panel 5 with non-glued carpets, for both panel and heavy layers, are presented in Figure 4.17. Each of the orange lines presents the RMS FRF for one of the four carpets. Each of the black lines presents the RMS FRF for the panel with one of the four carpets on top. Since the geometries of the carpets varies to some degree, the contact between panel and carpet also varies.

The RMS FRFs for the panel indicate a similar behaviour independent of which carpet that is placed on top. The resonance frequencies of the panel have a small variance over the whole frequency range. However, at some frequencies the amplitude of the panel response varies about 20 dB. So the variation in response can be rather large. The RMS FRFs for the carpets show a larger dispersion than the RMS FRFs for the panel, both in resonance frequencies and amplitude.

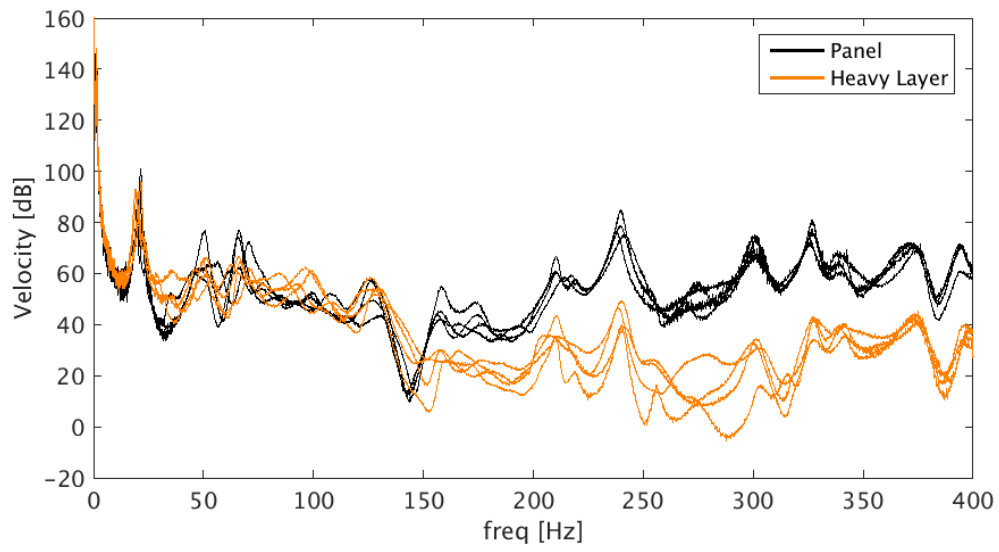


Figure 4.17: RMS FRFs for Panel 5 with non-glued carpets (Black lines) vs RMS FRFs for heavy layers of the non-glued carpets (orange lines).

5. Correlation of Numerical and Experimental Results

In this chapter, the numerical studies are presented and discussed. The objective was, 1) to evaluate the correlation between numerical results and measured data, and 2) to procure an understanding of the physical phenomena that governs the behaviour of the panel carpet–system.

For the measurements of panels with carpets, FRFs of panel-to-panel and panel-to-carpet were compared, between simulations and measurements. Two different modelling strategies were used to model the carpet: 1) model the carpet with NSM elements, and 2) model the carpet with solid elements. The difference between modelling strategies, and their correlation to measurements, in different frequency ranges was studied.

5.1 Correlation of Panel Without Carpet

It was concluded from the measurements of panels without carpet, that the dispersion of the dynamic response between the panel samples was low for the first resonance frequency, but increasing with frequency. Measured FRFs for each panel plotted vs the FRFs for the numerical model are presented in Figure 5.1. These results are representative for the remaining eight FRFs that were measured and calculated. Observing the results, it can be concluded that the calculated FRF seems to correlate quite well with the FRF of Panel 1 up to 200 Hz. As discussed in Chapter 1.4 four of five panels had a visible curvature in one of the corners, probably caused by the process of cutting them from a larger panel. The panel that had no visible curvature was Panel 1, which is a probable explanation for why the correlation to Panel 1 is the highest. However, the correlation seems to decline with frequency above 200 Hz. A possible explanation for this is that smaller imperfections influence the behaviour more at higher frequencies.

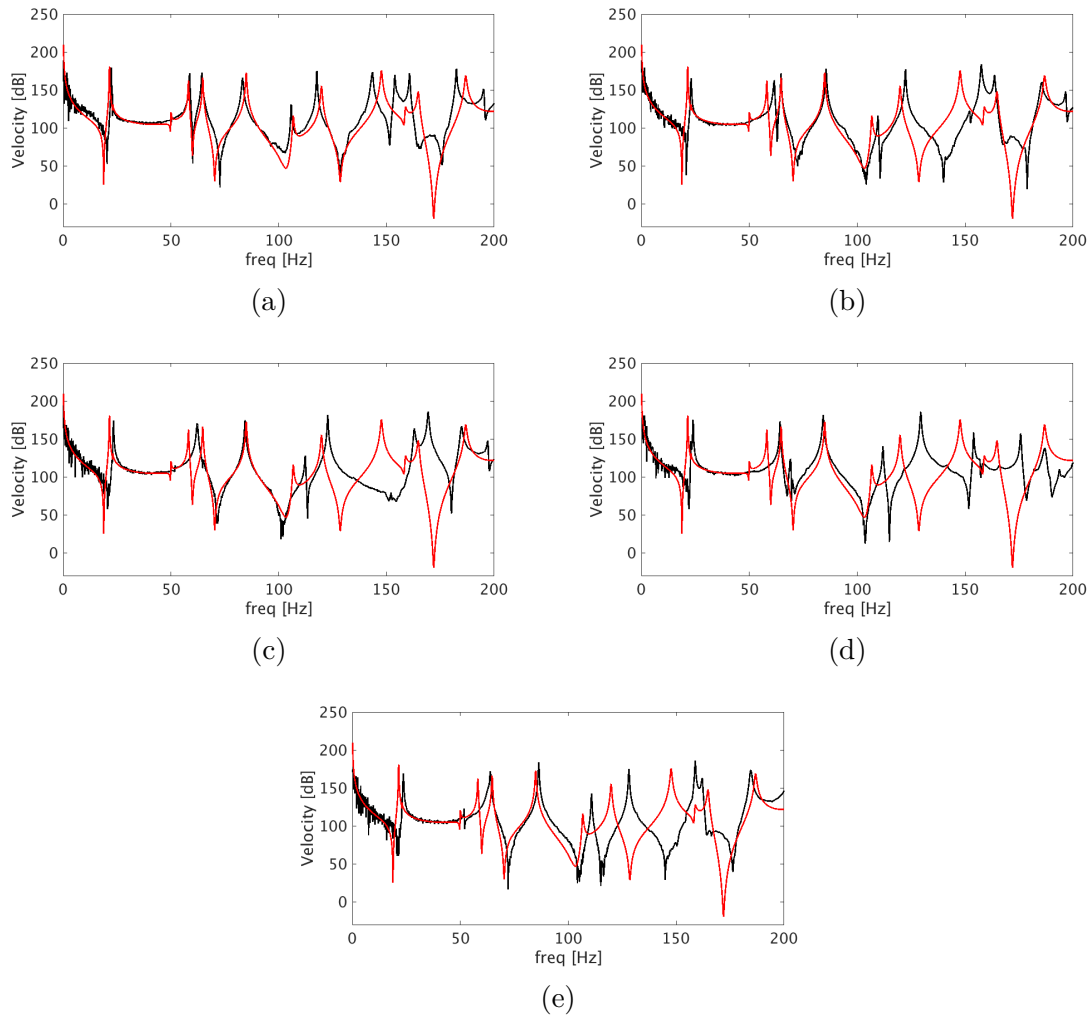


Figure 5.1: FRF for each panel (black) vs the same calculated FRF (red). (a) shows FRF for Panel 1, (b) shows FRF for Panel 2, (c) shows FRF for Panel 3, (d) shows FRF for Panel 4 and (e) shows FRF for Panel 5.

5.2 Correlation of Panel With Carpet

The correlation between the measurement results and numerical results are presented below. First in Chapter 5.2.1, the correlation between the measurement results of the panel with glued carpet and numerical results is presented. In Chapter 5.2.2, the correlation between the measurement results of the panel with non-glued carpet and numerical results is presented.

5.2.1 Glued Carpet

One hypothesis discussed in Chapter 1.1, was that the model with solid element representation of the carpet would correlate better with the panel with glued carpet. This reason was that the RBE3 connection is believed to behave more like a glued

than a non-glued connection. One reason for performing measurements on a panel with glued carpet was to evaluate the correlation to a model with the carpet modelled with solid elements connected to the panel with RBE3 elements. If the correlation is high, it is fair to assume that a solid model is detailed enough to represent the dynamic behaviour of a carpet. In Figure 5.2, RMS FRF 13, for both the numerical model and the measured panel with glued carpet is presented.

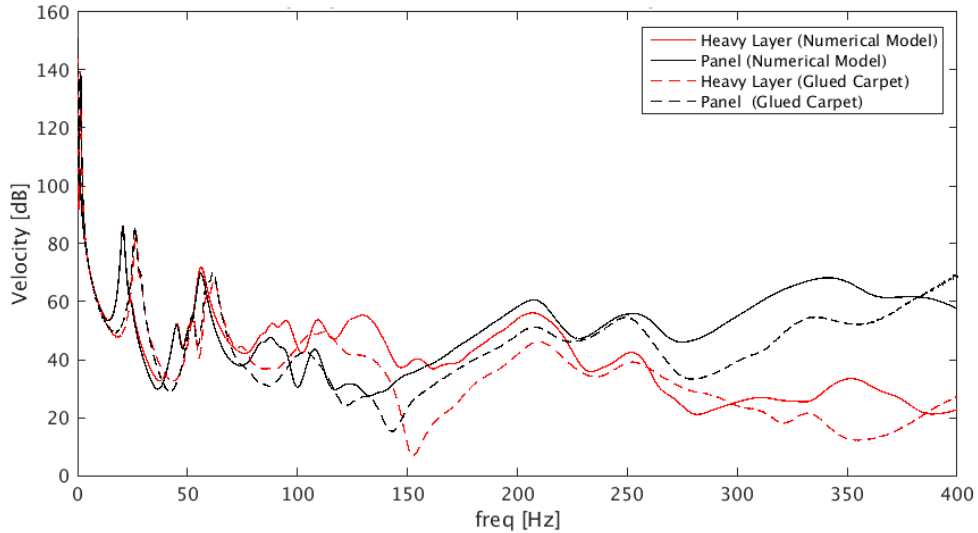


Figure 5.2: Numerical model vs measurements of panel with glued carpet.

There are a few interesting observations to be made from Figure 5.2. First, considering the frequency range 0–75 Hz, it seems as the curves of the numerical model is shifted to the left, compared to the measured curves. Otherwise, both amplitude and shape of the curves seems to be very similar. Secondly, it seems as the frequency range where the amplitude in the heavy layer is higher than the amplitude of the panel (75–150 Hz), is shifted. The final observation is that the difference in amplitude between panel and heavy layer is larger for the numerical model than for the physical model.

Despite the observed differences in the behaviour of simulations and measurements, the overall behaviour is similar. Simulations and measurements show the same characteristics. Both display an added mass behaviour, a resonant behaviour and a vibration isolated behaviour of the heavy layer. Approximately in the same frequency ranges. The characteristics of the curves are also similar.

5.2.2 Non-Glued Carpet

The carpets are in reality, generally not glued to the panels in the vehicle bodies. An effect of this is that the connection between panel and carpet is not fully known. This makes the modelling of the interface between panel and carpet complicated. It was not in the scope of the dissertation to investigate different modelling strategies of the connection. Hence, the measurements of the panel with non-glued carpets were

evaluated against the same numerical model as the panel with glued carpet. The numerical results vs the measurement results of panel with non-glued carpets are presented in Figure 5.3. As explained in Chapter 4, the measurements on the panel with non-glued carpets were performed with four different carpets. The measured RMS FRFs presented are the mean of those obtained for the four tested carpets.

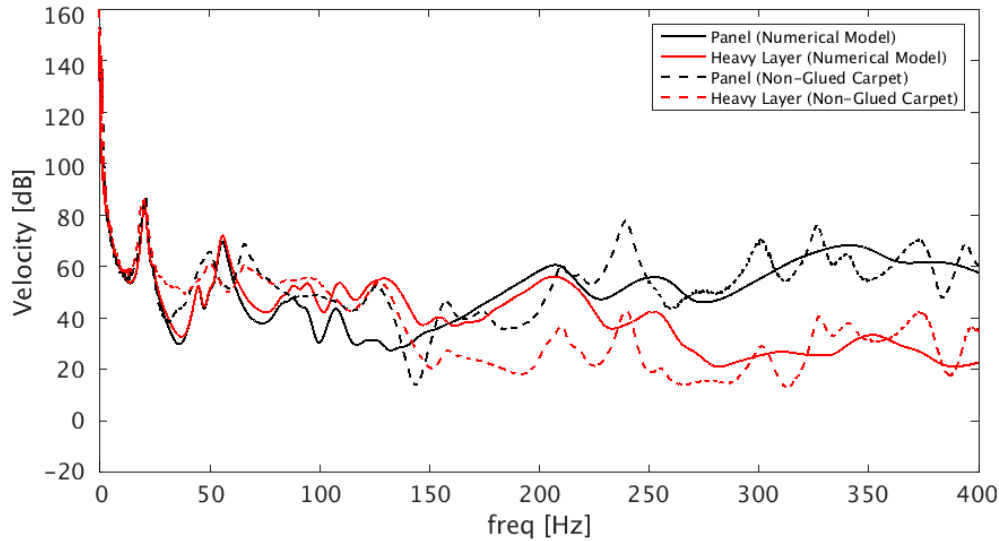


Figure 5.3: Numerical model vs measurements of panel with non-glued carpet.

It can be observed that there is no clear shift in the frequency of the first resonance, as could be seen in the correlation for panel with glued carpet. It can also be observed that the amplitude of both panel and heavy layer correlates better here. However, the measurements indicate that the measured example structure is less damped in the frequency range 150–400 Hz, than the numerical model.

5.3 Parametric Study

A parametric study was performed to increase the understanding of the model. It was also performed to see what properties of the model that might contribute to the inaccuracies, seen in the correlations. The parameters that were tuned were the stiffness of the foam and the stiffness of the heavy layer. The effect of tuning parameters was assessed by evaluating the ERP of panel and heavy layer for a model with solid element representation of the carpet.

5.3.1 Stiffness of Carpet

The effect of a stiffer carpet was evaluated. The stiffness of the carpet was increased by increasing the stiffness of both foam and heavy layer. This was done separately and analysed in one analysis each. That is, in the first analysis the stiffness of the

foam was increased by a factor 2 and the stiffness of the heavy layer. All other parameters were kept constant. Then, in the second analysis the stiffness of the heavy layer was increased by a factor 10 and the stiffness of the foam and all the other parameters were the same as in the original model.

The ERP of the model with stiffer foam vs the model with the original parameters is presented in Figure 5.4. In Figure 5.5, the ERP of the model with stiffer heavy layer vs the model with the original parameters is presented.

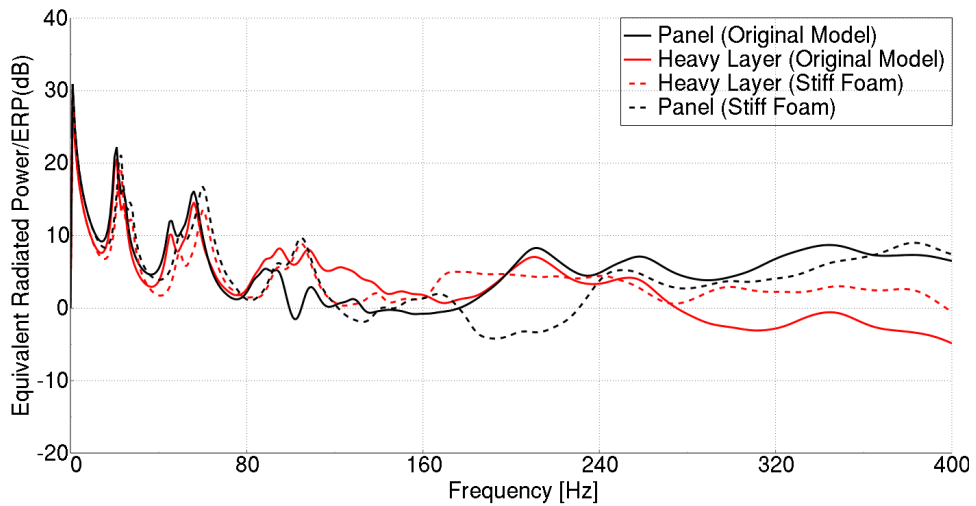


Figure 5.4: Model with original parameters vs model with increased stiffness of the foam.

The main observation to be made from Figure 5.4, is that the frequency range where the added mass behaviour can be observed, is extended by an increased stiffness of the foam. More specifically, the panel and the heavy layer curves follow each other up to 130 Hz for the model with stiffer foam. The curves for the model with the original stiffness of the foam, only follows each other up to 80 Hz. The frequency range where the heavy layer have a higher response than the panel is also wider for the model with stiffer foam. it can also be observed that the peaks of the curves up to 80 Hz have a slight shift upwards in frequency for the model with stiffer foam.

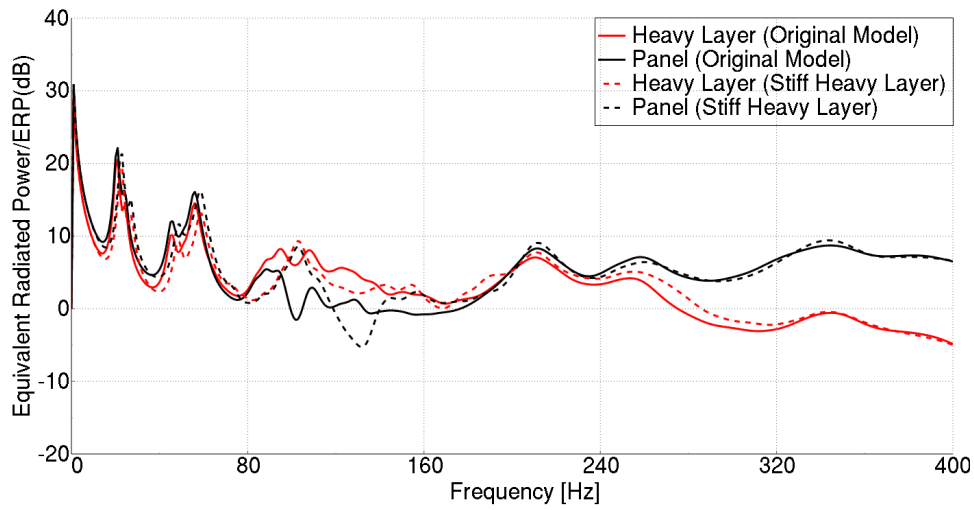


Figure 5.5: Model with original parameters vs model with increased stiffness of the heavy layer.

The effect on the vibrational response of panel and heavy layer are presented in Figure 5.5. The main observation to be made is that increasing the stiffness of the heavy layer by a factor 10, the frequency range where the carpet acts as an added mass is extended from 80 to 120 Hz. The frequency range where the response in the heavy layer is higher than the response in the panel is narrower when the stiffness of the heavy layer is increased. The frequency where the heavy layer starts to become vibration isolated seems to be unaffected by this increase of stiffness of the heavy layer.

6. Conclusions and Discussion

The aim of the dissertation was to provide knowledge of the dynamic behaviour of panels and carpets, to improve the modelling strategies used to predict acoustic pressure in vehicles. This was done by measuring the dynamic response of example structures composed of panels with and without carpets. The measurements were used to evaluate the dynamic behaviour of, and interaction between, panels and carpets. The correlation between measured results and numerical results was evaluated in order to evaluate numerical modelling strategies. A parametric study was also performed to investigate how different material parameters affected the dynamical behaviour of the analysed structure.

6.1 Main Observations

Considering the results presented in Chapter 4 and 5, a several observations are made. The main observations are listed below.

- Measurement results for the panel with glued carpet shows clear tendencies of the expected dynamic behaviour, discussed in Chapter 1.1. The measurement results for the panel with non-glued carpets does not show the same clear tendencies.
- A model with linear-elastic solid representation of the carpet shows clear indications of representing the vibro-mechanical phenomena that govern the dynamic behaviour of the panel with glued carpet in the studied frequency range. Further parameter calibration is needed to improve correlation.
- The variation in contact, caused by differences in the geometry of the carpets, for the non-glued carpets has quite small effect on the resonance frequencies of the panel, while amplitude levels are affected by as much as 20 dB.
- Gluing the carpet to the panel results in a response of the panel that is more damped and have lower amplitude, compared to the non-glued case. These are indications of that gluing the carpet adds stiffness to the panel.
- The NSM representation of the carpet is suitable for frequencies well below the measured heavy layer resonance, i.e. in the frequency range 0–75 Hz in the example case.

6.2 Discussion

Possible sources of error and the measurements that were used to evaluate the dynamic behaviour of the panels and carpets are discussed in the following sections.

6.2.1 Test Specimen

The panel cut-outs used in the study was cut out manually, from the original floor panels. This increased the probability of deviation between the panel cut-outs. It is reasonable to assume that, 1) the panels have not been cut identically which results in small deviations between the size and geometry of the panel cut-outs, and 2) there is a possibility that the panel cut-outs was deformed during the cutting process. The panel cut-outs were inspected ocularly to identify any visible deviations and damages. It was observed that four of five panel cut-outs (hereinafter referred to as the panels) had a visible curvature in one of the corners. The curvature was not identical in all the panels. It is believed to be a result of the manufacturing process or, more likely, the cutting process. It is also possible that other non-visible deformation were present. These differences in geometry is the most likely cause of the dispersion between the dynamic behaviour of the panels. The carpet cut-outs showed even larger variations in their geometries than the panels. This variations are probably what caused the dispersion between the measured RMS FRFs presented in Figure 4.17.

6.2.2 Evaluation of Measured Data

The response was measured in four points on the panels and in four points on the heavy layers, as explained in Chapter 4. The RMS FRF were than calculated based on these measured response. This is explained in more detail in Chapter 4.3. During the processing of the measured data the following observations were made:

- The measured response closest to the excitation point was generally much higher than the responses measured in points further away.
- Excluding the FRF with the highest amplitude in the calculation of the RMS FRF, drastically changes the characteristics of the RMS FRF, compared to the RMS FRF based on all four FRFs.

The response measured closest to the excitation point was significantly higher than the other three responses measured. This caused the FRF measured between the point closest to the excitation and the excitation point (hereinafter referred to as the dominant FRF) to be dominant in the RMS FRF. More specifically, there is a strong resemblance between the dominant FRF and the RMS FRF composed of all four FRFs. An example of this is the RMS FRFs presented in Figure 4.15. Plotting just the FRFs for an excitation in point 13 and the response measured in point 13 of panel and heavy layer, will give almost the same appearance. The other observation that was made was that if the dominant FRF was excluded from the

RMS FRF, the characteristics of the RMS FRF change drastically. This RMS FRF did not show the same tendencies of the expected behaviour, discussed in Chapter 1.1.

This is a problem since the RMS FRFs were used as an indication of the general response of a surface. This problem could have been avoided by measuring the response in more points, and include more FRFs in the RMS FRF calculation. If more points closer to the excitation point were incorporated in the measurements, perhaps not only one FRF would dominate the RMS FRF.

However, the data that is presented in Chapter 4 and 5 was specifically selected. More data was evaluated but not presented. Choosing what data to present necessitates causation, or it can otherwise be deceptive. For instance, the RMS FRFs were used to evaluate the dynamic behaviour of panels and carpets for an excitation in one of two points. It was chosen to only present the RMS FRFs for an excitation in one of the points. This data showed the clearest tendencies of the expected behaviour, explained in Chapter 1.1. The dynamic behaviour shown by the other RMS FRFs, which is not presented, did not show as clear tendencies of the expected behaviour. Considering the RMS FRFs for both excitation points, the tendencies of the expected behaviour are not as obvious, as only considering the RMS FRFs that are presented in Chapter 4. This observation indicates that the behaviour observed in the measurements are dependent of the point of excitation. Further investigations of how the excitation point affects the behaviour is therefore needed. This would ensure that the behaviour seen in the measurements presented in Chapter 4 is general for all excitation points.

6.2.3 Accuracy of Numerical Model

The model that was used in the correlation studies presented in Chapter 5 was created from a CAD model. Comparing the geometries of the numerical model and the specimen, differences were observed. The foam layer of the numerical model is overestimated by 5-10 mm in some areas, and the heavy layer is overestimated by approximately 3 mm across the whole surface. Despite this, the mass of the numerical model corresponds well with the weight of the example structures. It has not been established what causes the masses to correspond well despite that the geometries differ. However, it is probably due to that the material parameters used in the numerical model does not correspond to the material parameters of the example structure.

The value of evaluating the correlation between measurements and simulations, when the numerical model has such obvious deficiencies can be questioned. It is obvious that the correlation between the two would not be as good as a more correct model. However, despite the deficiency of the numerical model, it is still possible to draw conclusions regarding the abilities of the modelling strategies, and to provide recommendations on how to model carpets on panels.

An interesting observation is that even though the resemblance between the numerical model, used in the correlation studies, and the physical test specimen is poor, the correlation is quite good. This indicates that the behaviour seen might be

a quite general behaviour of this type of panels and carpets. That general material parameters for foams and rubber does not effect the characteristics of the behaviour to any large extent.

6.2.4 Damping

Modal damping was used in the numerical analyses. The damping ratio was set to 0.08 over the whole frequency range. It was decided by evaluating different damping ratios. Since the damping of the physical structure most likely is frequency dependant, a constant damping over the whole frequency range is a rough simplification.

It was seen in the dispersion measurements of the panels that the damping varied a lot, both between the modes of a panel, but also between the same mode of different samples. One have to consider that the geometries of the panels most likely were slightly altered in the cutting process, which probably affected the behaviour and modal properties of the panels. The carpets might not be damage by the cutting process, but the default dispersion between them is likely to be greater than the dispersion between the panels. Hence, an even larger dispersion in the damping between modes and specimen is likely for the panels with carpets. It might be possible to see some trends or tendencies in the damping though, which might can be used to model a frequency dependent damping. This would likely improve the correlation between numerical results and measurements. However, what type of damping that would generate the best correlation is needed to be investigated further.

6.2.5 Adding Stiffness by Gluing

As mentioned in Chapter 5.2, one of the observations of Figure 5.2 was that the first eigenfrequencies of the numerical model seemed to be approximately 7 Hz lower than the measured resonance frequencies of the panel with glued carpet. However, this is not the case if the numerical model is compared to the measurements of the panel with non-glued carpets. Here, the first resonance-/eigenfrequency seems to correspond well to each other. Since the variation in mass of the carpets is only some few percent, it is likely to be an increase in stiffness in the panel with glued carpet that is the reason for the shift of the resonance frequencies.

Another observation was, that for the panel with non-glued carpet, adding the carpet decreased the resonance frequency of the first mode of the panel. It is the opposite in the case for the panel with glued carpet. For this case the carpet seems to increase the resonance frequency of the first mode. Since the mass of both panels with carpets are approximately the same, it have to be a change in stiffness that causes the shift in resonance frequency. Hence it is reasonable that gluing the carpet to the panel caused the increased stiffness of the panel. With the same argument it was also reasonable that the RBE3 connection in the numerical model is unable to represent the stiffness of a glued connection.

6.3 Proposals for Future Work

As discussed in Chapter 1, the work done in the master's dissertation serves to increase the accuracy of acoustic pressure prediction in vehicles. The dissertation aimed to increase the knowledge of the vibro-mechanical behaviour of panels and carpets, which is considered essential for predicting the noise radiation from the panels. While the observations discussed in Chapter 6.2 provide important knowledge, further investigations are needed.

In order to verify the results obtained in this dissertation a larger data selection is necessary. Instead of measuring the response of panel and carpet with accelerometers, using a laser doppler vibrometer (LDV) would allow the response to be measured in a significantly larger amount of points. Measuring the response using a LDV also allows for measurements with no interference from accelerometer. Further, the validity of the measurements done on the example structure in this dissertation to a complete vehicle body is unknown. The dynamic behaviour of panel and carpet in a vehicle body should therefore be investigated.

It has been shown in this dissertation that gluing the carpet to the panel decreases the response in the panel. Since the panels are a major contributor to interior noise, it is likely that gluing the carpets in vehicles would decrease the interior noise. If this is the case, gluing the carpets would be a relatively easy way to improving the NVH performance in vehicles. Hence, further investigation is needed to evaluate the potential benefits of glued carpets on interior noise levels.

When the vibro-mechanical behaviour of panels and carpets is better understood, the next step is to investigate the sound radiation of these. It is of interest to understand whether the heavy layer radiates sound or if it is only the panel. If the heavy layer also radiates sound, it is important to know in what frequency ranges this is important to consider. More specifically, it is of interest whether the high vibration amplitudes of the heavy layer around 100–150 Hz, seen in this dissertation, is a problem or not. This would be an important step in a better understanding of sound radiation of panels and carpets.

The suggestions above are an extension of the experimental analysis. However, there are some proposals that could be seen as an extension to the numerical work presented in this report. The foam in the carpets are in fact not an isotropic solid, but a poro-elastic material. Thus, it can be questioned whether a poro-elastic material model would allow for better correlation with the measurements. It is believed that a poro-elastic material model would be able to represent the dynamic behaviour in the higher frequency range with higher accuracy than a isotropic model, but further investigations is needed. Additionally, the modelling strategy used to model the connection between panel and carpet in this work is believed to be a major source of error for the correlation between measurements and numerical model. Therefore, further investigations of how to model the connection are needed.

Bibliography

- [1] Barry Wyerman et al. *Automotive noise and vibration control practices in the new millennium*. Tech. rep. SAE Technical Paper, 2003.
- [2] Arnaud Duval et al. “Trim FEM simulation of a dash and floor insulator cut out modules with structureborne and airborne excitations”. In: *Journal of the Acoustical Society of America* 123.5 (2008), p. 3532.
- [3] Christopher J Cameron, Per Wennhage, and Peter Göransson. “Prediction of NVH behaviour of trimmed body components in the frequency range 100–500 Hz”. In: *Applied Acoustics* 71.8 (2010), pp. 708–721.
- [4] Toru Yamazaki et al. “Modeling of Floor Carpet on Vibration and Structure-Bone Noise Transmission”. In: *ICA2004, Proceedings of ICA2004, IV-2923-2926* (2004).
- [5] Claudio Bertolini et al. *FE Analysis of a Partially Trimmed Vehicle using Poroelectric Finite Elements Based on Biot’s Theory*. Tech. rep. SAE Technical Paper, 2007.
- [6] Niels Saabye Ottosen and Matti Ristinmaa. *The mechanics of constitutive modeling*. Elsevier, 2005.
- [7] Frank Ihlenburg. “Sound in vibrating cabins: Physical effects, mathematical formulation, computational simulation with fem”. In: *Computational Aspects of Structural Acoustics and Vibration*. Springer, 2008, pp. 103–170.
- [8] Thomas G Carne and Clark R Dohrmann. “Support conditions, their effect on measured modal parameters”. In: *PROCEEDINGS-SPIE THE INTERNATIONAL SOCIETY FOR OPTICAL ENGINEERING*. Vol. 1. SPIE INTERNATIONAL SOCIETY FOR OPTICAL. 1998, pp. 477–483.
- [9] Thomas G Carne, D Todd Griffith, and Miguel E Casias. “Support conditions for experimental modal analysis”. In: *Sound and Vibration* 41.6 (2007), pp. 10–16.
- [10] Kenneth G McConnell. “The elusive free-free boundary condition”. In: *Proceedings of the XXXV International Modal Analysis Conference, Garden Grove, CA*. 2016.

A. Repeatability

The variations in the experimental measurement setup are shown in the figures below.

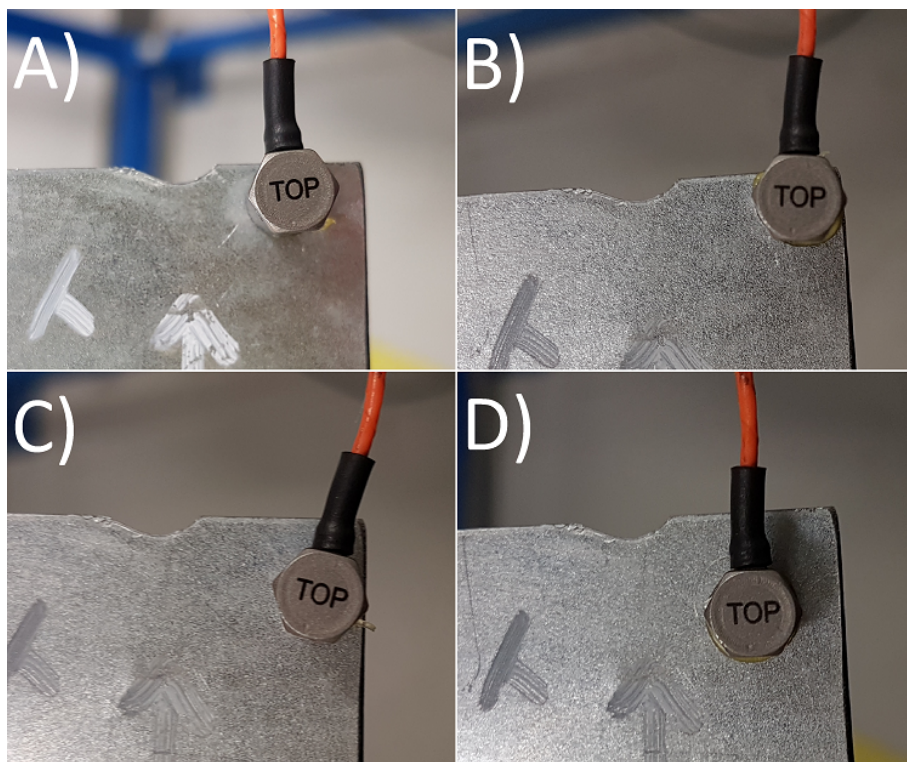


Figure A.1: Accelerometer positions used in the measurements to evaluate the effect of small variations of accelerometer position.

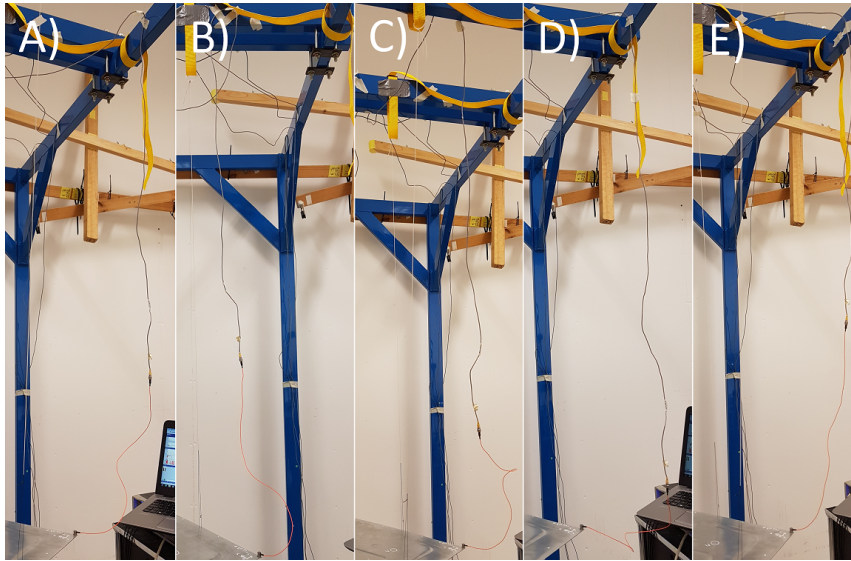


Figure A.2: Cable suspensions used in the measurements to evaluate the effect of different cable suspensions.

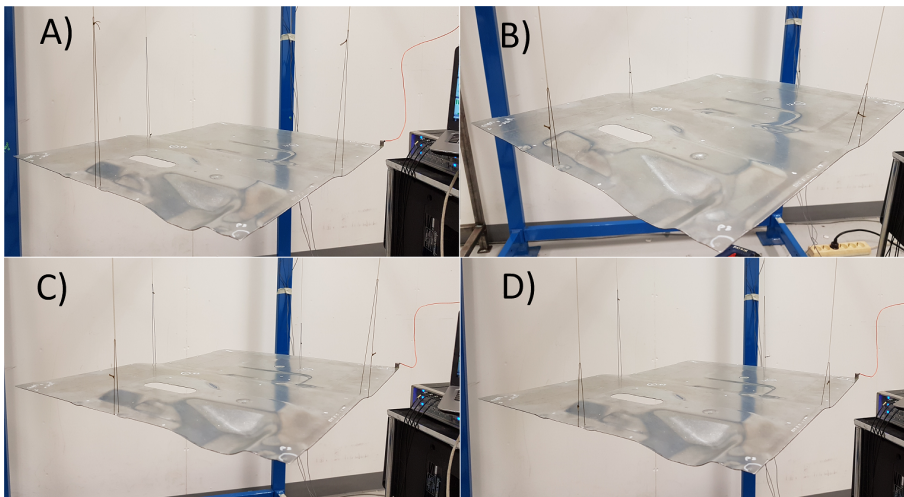


Figure A.3: Thread lengths used in the measurements to evaluate the effect of variations of thread length.

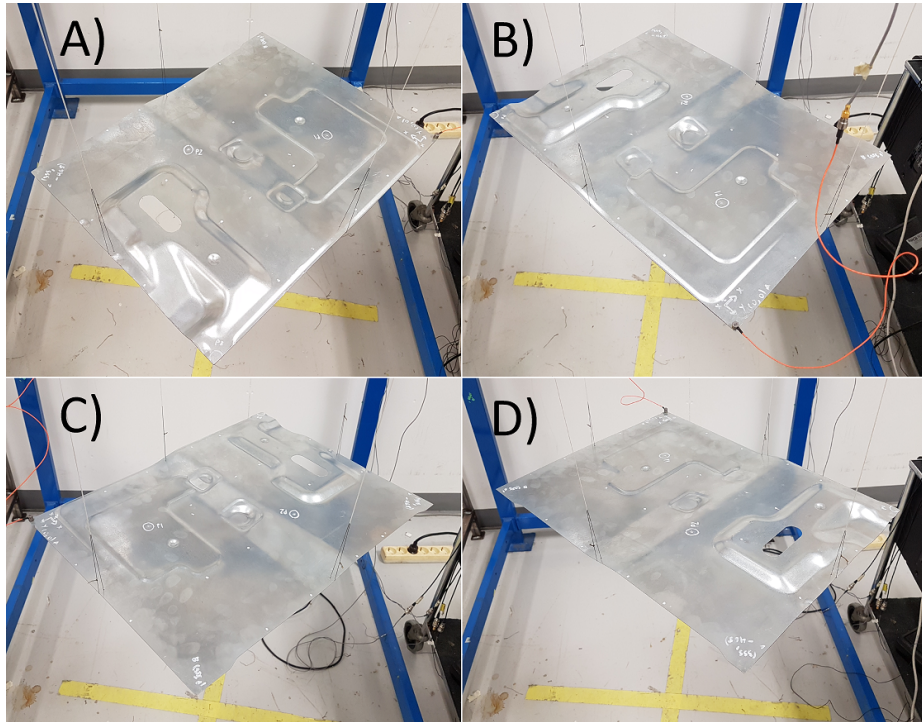


Figure A.4: Panel rotations used in the measurements to evaluate the effect of rotation of panels.